metals

MDPI

Review

Using Ball Milling for Modification of the Hydrogenation/Dehydrogenation Process in Magnesium-Based Hydrogen Storage Materials: An Overview

Jinzhe Lyu *, Andrey Lider and Viktor Kudiiarov

Division for Experimental Physics, School of Nuclear Science and Engineering, National Research Tomsk Polytechnic University, Lenin Ave. 43, Tomsk 634034, Russia

* Correspondence: czinchzhe1@tpu.ru; Tel.: +79234234577

Received: 23 May 2019; Accepted: 29 June 2019; Published: 9 July 2019

Abstract: Magnesium-based hydrogen storage materials are considered to be one of the most promising solid-state hydrogen storage materials due to their large hydrogen storage capacity and low cost. However, slow hydrogen absorption/desorption rate and excessive hydrogen absorption/desorption temperature limit the application of magnesium-based hydrogen storage materials. The present paper reviews recent progress in improving the hydrogen storage properties by element substitution and additives. Ball milling is the promising technology for preparing magnesium-based hydrogen storage materials. The research and development of approaches for modifying magnesium-based hydrogen storage materials prepared by ball milling is systematically expounded. It is concluded that ball milling can significantly improve the kinetic and electrochemical properties of magnesium-based hydrogen storage materials and increase the hydrogen storage capacity. In the future, the research of magnesium-based hydrogen storage materials should be developed in terms of hydrogen storage mechanism, computer design of materials and development of a more optimized catalytic system.

Keywords: magnesium-based hydrogen storage materials; element substitution; additive; ball milling

1. Introduction

As a very important functional material, hydrogen storage materials play an irreplaceable role in the field of secondary energy, especially in the research of fuel cells and rechargeable batteries. The study of hydrogen storage materials is directly related to the application of electric vehicles, and also has an important impact in submarines, spacecraft and other applications. Various hydrogen storage materials have been developed worldwide [1–15], and many researchers have focused their research on the study of magnesium-based hydrogen storage materials. Much attention is paid to the study of magnesium-based materials due to the fact that magnesium has many important properties. First of all, magnesium is one of the most abundant elements in the earth's crust, ranking the 8th, accounting for 2.35% of the crustal mass. Secondly, magnesium has large hydrogen storage capacity, theoretical value of which can reach 7.6wt% [16–19]. However, as a hydrogen storage material pure magnesium has poor kinetic performance for hydrogen absorption/desorption, conditioned by the following: (1) existence of oxide on its surface, (2) slow diffusion rate of hydrogen in the bulk MgH_2/Mg, (3) with poor decomposition of hydrogen on the Mg surface [20] the rate of hydrogen absorption/desorption is very low, and the hydrogen desorption temperature is relatively high. To achieve an acceptable rate of hydrogen desorption, the desorption temperature must be above 350 °C, which makes the application of magnesium difficult.

The methods of hydrogen storage materials preparation have significant influence on the hydrogen storage properties. Widely used methods include hydriding combustion synthesis, melting method, sintering process, ball milling etc. Ball milling is an important structural modification method developed in the 1980s. Compared with ball milling, other methods mentioned above possess certain limitations to be considered. For example, in spite of the hydrogen storage materials prepared by the hydriding combustion synthesis having high hydrogen absorption/desorption activity and defect density, the hydriding combustion reaction is complicated, the experimental repeatability is poor, and the granularity of reaction products is irregular [21]. Therefore, the hydriding combustion synthesis often needs to be combined with ball milling. The melting method has strict requirements on the melting point of the metal elements of the hydrogen storage alloy [22]. Mechanical alloying based in ball milling has unique advantages for preparation of alloys with large difference in melting points. Mechanical alloying, with no need to heat and completely relying on mechanical action, enables not only easy control of the composition of the alloy, but also allows to directly obtain the materials with metastable structure such as nanocrystalline structure, amorphous structure and supersaturated solid solution. In terms of material preparation methods, ball milling is the main method for preparing magnesium-based hydrogen storage alloys and can cause interdiffusion and alloying reactions between different elements to produce alloys with micron- or even nano-size grains. For the research purposes, ball milling preparation and nanocomposite are one of the main ways to improve the hydrogen absorption/desorption properties of magnesium-based hydrogen storage alloys. This is due to the fact that ball milling introduces a large number of defects and grain boundaries in magnesium-based hydrogen storage alloys. Moreover, magnesium-based hydrogen storage alloys prepared by ball milling are usually nano-size multiphase system, a large number of interfaces in which and the above-mentioned defects and grain boundaries provide significant channels for the diffusion of hydrogen atoms between grains. In addition, ball milling leads to significant reduction of grain size, thereby accelerating the diffusion of hydrogen atoms inside grains [23–29]. Theoretically ball milling can break the oxide layer on magnesium powder and provide fresh surfaces [18], however, because of the limitation of the vacuum degree of the ball-milled vial, nanocrystalline Mg always interacts with oxygen during ball milling, especially during hydrogen absorption/desorption cycles, which lead to the oxygen layer reform [30]. In this paper, we paid especial attention to the substitution and additive-enhanced MgH_2 and compared the effects of different modification methods and the modification mechanisms in as much detail as possible. Reviewing this data, we presume this paper can assist in better understanding of MgH_2, and shape perspectives for further research.

2. Ball Milling Modification of Mg-Based Hydrogen Storage Alloys

2.1. Modification by Element Substitution of Mg_2Ni

The hydrogen storage capacity of Mg_2Ni is 3.6%, and it is necessary to release hydrogen gas above 200 °C. Mg_2Ni belongs to A_2B type hydrogen storage alloy, A is a hydrogen-absorbing element or an element with a strong affinity for hydrogen. A usually belongs to IA-VB group metal elements, such as Ti, Zr, Ca, Mg, V, Nb, Re (Rare earth element) etc., reaction of which with hydrogen is exothermic (ΔH <0). B is the element that absorbs little hydrogen or no hydrogen at all. B is usually Fe, Co, Ni, Cr, Cu, Al etc., reaction of which with hydrogen is endothermic (ΔH > 0). A element controls the hydrogen storage capacity, while B element controls the reversibility of hydrogen absorption/desorption and regulates the equilibrium pressure of hydrogen desorption [31–33]. Element substitution and changing the proportions of elements are the common method for improving the properties of magnesium-based alloys, the core of which is to adjust the hydrogen absorption capacity and hydrogen absorption/desorption properties of the hydrogen storage alloy by adjusting the proportion and type of A and B element. The purposes of element substitution of Mg_2Ni are as follows: (1) improving hydrogen desorption pressure; (2) reducing hydrogen desorption temperature; (3) improving hydrogen absorption/desorption rate. The purposes can be realized due to the fact

that the endothermic metal in the hydrogen storage alloy is able to control the reversible process of hydrogen absorption/desorption. The existing element substitution methods in the literature can be summarized as follows: (1) Substitution of Mg with an element that is more electronegative than Mg to reduce the stability of the hydride and improve the reversibility; (2) Substitution of Ni with an element, which radius is larger than that of Ni; (3) Substitution of Mg and Ni with various elements.

2.1.1. Modification by Substituting Mg Element

Substitution of Mg element was carried out experimentally, basically by using one or two of Al, Ti, V, Zr, Ag, Pd, Co and other metal elements [34–43].

After substituting part of the Mg elements in the Mg_2Ni alloy with Ag, it was found that the new alloy had lower hydrogen desorption temperature, absorbing hydrogen at 423 K without any activation, and the hydrogen absorption capacity was also reduced. This can be explained due to the substitution of Mg leading to reduction of the absolute value of the enthalpy [44,45].

The experimental results of substitution of Mg element with Al showed that with increase of the addition of Al the hydrogen storage capacity of the alloy will be reduced. This is due to the substitution of Mg with Al, which reduces the formation of the hydrogen absorbing phase Mg_2Ni. However, the addition of Al element will increase the hydrogen absorption/desorption rate of Mg_2Ni hydrogen storage alloy compared with that before substitution. Furthermore, the hydrogen absorption temperature of the alloy decreases with the increase of Al%, and the addition of Al can effectively improve the discharge capacity and cycle stability. Several possibilities explaining the prominent effect of Al additives on the hydrogen storage properties of Mg_2Ni were considered [46–50]: (1) the addition of Al element leads to formation of non-hydrogen-adsorption phase Al_3Ni_2 and hydrogen-adsorption phase Mg_3AlNi_2 in the Mg_2Ni hydrogen storage alloy, these new phases increase grain boundaries and defects in the alloy, which provide significant hydrogen diffusion channels; (2) The synergistic hydrogen absorption effect of Mg_3AlNi_2 and Mg_2Ni can significantly improve the hydrogen absorption/desorption properties of the alloy; (3) After the Al element is added, a dense layer of Al_2O_3 is formed on the surface of the alloy, and the corrosion resistance of the alloy is also enhanced, thereby the cycle life of the alloy is prolonged. These explanations were also confirmed by the research results of Xue et al. [51] and Yuan et al. [35].

The hydrogen absorption/desorption properties of Mg_2Ni at low temperatures (below 300 °C) can also be improved by substituting Mg with Ti. The work of Liang et al. [52] has certain representativeness. $Mg_{1.9}Ti_{0.1}Ni$ nanoalloy was prepared by substituting Mg element with Ti element. The alloy had stable hydrogen absorption/desorption properties and quickly absorbed hydrogen at 200 °C without any activation. Further to that, at 150 °C 3 mass% absorption was achieved within half an hour. Iwakura et al. [53] prepared $Mg_{1.9}Ti_{0.06}V_{0.04}Ni$ by partially substituting Ti element in $Mg_{1.9}Ti_{0.1}Ni$ with V element. It was found that compared with substitution of Mg with a single Ti element or V element substitution of Mg element simultaneously with Ti and V elements exhibited further improved cycle performance. Improvement of the hydrogen absorption/desorption properties and cycle stability of the alloy by Ti element can be explained by Ti element forming an oxide film on the surface of the alloy, which restrains further oxidation of the Mg element, and at the same time forms a nickel-rich layer on the surface of the alloy, thereby improving the cycle stability of the alloy [54].

Substituting Mg with Zr is also one of the ways to improve the hydrogen storage properties of Mg_2Ni. Substituting Mg with Zr allowed not only improve the hydrogen desorption properties of the alloy electrode at 30 °C, but also enhanced the hydrogen absorption/desorption capacity of the alloy at low temperatures (30 °C and 200 °C) [55]. Goo and Lee [56] attributed the enhanced hydrogen absorption capacity of the Mg-Ni-Zr alloy to the increase of the atomic spacing in the alloy and the increase of the active point, which promoted the hydrogen dissolve ability of the alloy. Feng et al. [57] believed that the proper addition of Zr can improve the corrosion resistance of the alloy, but maximum discharge capacity of the alloy can be probably reduced.

In addition, the substitution of Mg in Mg_2Ni with Re elements can also improve the hydrogen storage properties of Mg_2Ni series alloys to certain extent [55].

2.1.2. Modification by Substituting Ni Element

Substitution of Ni element experimentally were carried out basically by using one or two of Ti, Cr, V, Fe, Cu, Co, Zn, Pd, W, Mn etc. to improve the hydrogen absorption/desorption reversibility of Mg_2Ni series alloys [58–64].

Yang et al. [64] prepared $Mg_2Ni_{0.75}M_{0.25}$ alloy by substituting Ni element with M (M = Ti, Mn, Co, Cr, Zn, Cu, Fe) and investigated their hydrogen storage properties. The results showed that the substitution of Ni with Mn, Co, Cr leaded to obvious reduction of the decomposition equilibrium pressure of Mg_2Ni, while the substitution with Ti element and Cu element caused increase in the equilibrium pressure, with regard to Zn element and Fe element, with their little effect on the results observed.

Zhang et al. [65] prepared $Mg_2Ni_{1-x}Zr_x$ alloy by substituting Ni element with Zr element. It was found that the main phase of the alloy was a hexagonal structure as that of Mg_2Ni and with the gradual increase of the Zr element content the hydride formation heat was gradually reduced, and the hydrogen desorption temperature was also lowered. Compared with Mg_2Ni alloy it was also found that the hydrogen desorption capacity of the substituted with Zr alloy increased at 340 °C and under the pressure of 1 atm.

Pd has a large catalytic activity for the hydrogen absorption/desorption of alloys and is a suitable additive for mechanical ball milling. The dispersed in Mg_2Ni nanosized Pd particles play a catalytic role for the hydrogen absorbing reaction, thereby improving the hydrogen storage properties of the alloy. However, as the Pd content increases, the hydrogen storage capacity of the alloy decreases. The reason for this lower hydrogen capacity is still not clear and may be related to slower hydrogen diffusion through the initially formed layer of Mg_2NiH_x [66,67].

Of all works on partial substitution of element Ni with Cu, the work of Chen et al. stands out. The researchers found that with the increase of Cu content, the alloy formed Mg_2Cu phase and $Cu_{11}Mg_{10}Ni_9$ phase. Besides, the results of their research showed that the addition of Cu allows to increase the hydrogen desorption equilibrium pressure that is consistent with the findings of Yang [64] et al., but leads to reduction of hydrogen storage capacity of the alloy. Two possibilities explaining the effect of Cu additives on the hydrogen storage capacity of Mg were considered: (1) Since the atomic radius of Cu is larger than Ni, the substitution of Ni with Cu leads to decrease in the material density, the volume expansion ratio after hydrogen absorption, and thereby the hydrogen storage capacity; (2) The production of new phase $Cu_{11}Mg_{10}Ni_9$ reduces the formation of hydrogen absorption phase Mg_2Ni. In spite of the negative effect of Cu additive on the hydrogen storage capacity of the alloy, it should be noted that adding Cu element can effectively improve discharge capacity and cycle stability [68,69].

2.1.3. Modification by Substituting Mg and Ni Element

Experiments have also been conducted on the partial substitution of elements on both sides of A and B in Mg-Ni series alloys. Generally, new phase structures are formed. Xie et al. reported microstructure of the $Mg_{1.8}Al_{0.2}Ni_{0.8}Cr_{0.2}$ alloy, obtained by simultaneous substituting Mg and Ni with Al and Cr respectively. It was found that there is a synergistic effect between Al and Cr additives: Cr has the ability to inhibit the formation of non-hydrogen-adsorption phase Al_3Ni_2, and simultaneously facilitates the formation of hydrogen-adsorption phase Mg_3AlNi_2; similarly, Al can inhibit the formation of non-hydrogen-adsorption phased −[Cr, Ni], such microstructure of $Mg_{2-x}Al_xNi_{1-y}Cr_y$ alloy is beneficial to hydrogen storage capacity and cyclic stability [47].

Wang et al. [70] prepared the $Mg_{2-x}Ti_xNi_{0.8}Cr_{0.2}$ (x = 0.05, 0.10, 0.15, 0.20) alloy by substituting Mg with Ti and substituting Ni with Cr. The results showed that after Ti substituted Mg, there were two main phases Mg_2Ni and Ni and the trace amount of Mg and TiNi phases in the alloy. The TiNi phase

was dispersed in the alloy and had a certain catalytic effect on the hydrogen absorption/desorption properties of the alloy. The more Ti content is in the alloy, the faster the hydrogen desorption rate of the alloy is. However, with the increase of Ti content the hydrogen desorption capacity was reduced. This is due to the reduction of Mg content in the alloy, which leads to the reduction of the absolute enthalpy of the hydride. Duan et al. [71] investigated the structure and properties of $Mg_{1.5}Al_{0.5}Ni_{1-y}Co_y$ and found that when $y = 0.2$, the alloy capacity retention rate was optimal and the hydrogen desorption equilibrium pressure was the highest and widest. The hydride decomposition enthalpy of $Mg_{1.5}Al_{0.5}Ni_{0.8}Co_{0.2}$ alloy is -39.45 kJ/mol H_2, i.e., the hydride stability of the alloy increases after Co substitutes Ni.

2.1.4. Mg-Ni Series Alloys

In order to further improve the cycle life of Mg-Ni series hydrogen storage alloys while maintaining their high hydrogen storage capacity, in recent years, scientists have been using mechanical alloying method to prepare stoichiometry or non-stoichiometric Mg-Ni series amorphous alloys and progressed in research of the substitution modification of alloy elements [11,72,73]. Elements, widely used for alloying with Mg-Ni series materials, are V, Ti, Co and rare earth elements.

Zhu et al. [74] used Hydriding Combustion Synthesis (HCS) and Balling Milling technology to prepare $Mg_{90}Ni_{10-x}V_x$ ($x = 0, 2, 4, 6, 8$) alloys. It was observed that the hydrogen absorption properties of Mg-Ni-V alloy were better than that of binary Mg-Ni alloy. This is explained by the fact that the addition of V promotes the hydrogenation of Mg to some extent. While the hydrogen desorption properties of Mg-Ni-V alloy were inferior to that of binary Mg-Ni alloy, which can be explained by the fact that during hydrogen desorption the catalytic effect of Mg_2Ni is better than V, with the increase of V content in the alloy the content of VH_y phase gradually increased, while the content of Mg_2NiH_4 and $Mg_2NiH_{0.3}$ gradually decreased.

Ti alloying is one of the hot research in recent years. The doping of Ti can weaken the interaction between H atoms and Ni atoms, reduce the hydrogen absorption reaction enthalpy of the alloy system, and improve the hydrogen-decomposing ability of the hydride of Mg_2Ni [75]. However, the doping of Ti can also lead to the reduction of hydrogen storage capacity of Mg-Ni series alloys, Wang et al. [76] suggested that this may be related to the $TiNi_2$ phase appearing in the Mg-Ni-Ti alloy, which is not conducive to the gaseous hydrogen absorption of the alloy. Although the doping of Ti leads to decrease in the hydrogen storage capacity of Mg-Ni series alloys, the amount of MgH_2 formed by doping Ti is the highest compared to the doping of Ni and Nb into the Mg-Ni system [77], which suggests that Ti allows to commendably improve hydrogen storage properties of Mg-Ni series alloys.

Similarly, Co alloying can well improve hydrogen storage properties of Mg-Ni series alloys. Grigorova et al. [78] reported that the composites 85%Mg–15%$Mg_2Ni_{1-x}Co_x$ ($x = 0, 0.1, 0.3$) preserved high absorption capacity with decreasing temperature (4 wt% H_2 at the hydriding temperature of 423 K). Similar results have been observed by Zhao et al. [79].

Sun et al. prepared $Mg_{22}Y_2Ni_{10}Cu_2$ + x%Ni ($x = 0, 50, 100, 150$; mass fraction) composite materials with different ball milling time (10, 20, 30, 40 h) and analyzed the effects of milling time and nickel addition on the hydrogen storage properties of $Mg_{22}Y_2Ni_{10}Cu_2$ alloy. The results showed that ball milling improved the microstructure of the alloy and promoted the formation of amorphous and nanocrystalline in the alloy, besides, the addition of nickel significantly promoted the progress of the above process, so that the content of amorphous and nanocrystalline in the composite material greatly increased. The improvement of cycle stability was also obvious: S_{20} of the ball-milled for 20 h sample with composited nickel $x = 150$, was up to 80%. In addition, nickel, coated on the surface of the alloy, improved the surface activity of the alloy and effectively improved the overall hydrogen storage properties of the alloy [80].

The influence of elements such as Fe [81] and different Ni content [82] on hydrogen storage properties and electrochemical properties of Mg-Ni series alloys has also been reported in literature. These elements all improve the above properties of the alloy to varying degrees.

Details of the investigation results of the part of the above selected works on modification by element substitution of Mg_2Ni are presented in Table 1.

Table 1. Hydrogen storage properties of various Mg_2Ni alloys modified by element substitution.

Material	Rotation Speed, rpm	Time, h	Atmosphere	Ball-to-Powder Weight Ratio	Hydrogen Storage Properties	Ref.
$Mg_{1.8}Ag_{0.2}Ni$	400	2	0.2 MPa Ar	-	Abs: 2.5wt%/0.2 atm/200 °C $\Delta H_{abs} = -51.96$ kJ·mol^{-1}·H_2 $\Delta S_{abs} = -2.24$ J mol^{-1}·K^{-1} H_2	[45]
$Mg_2Ni_{0.9}Zr_{0.1}$	300	2	Ar	20:1	Des: 3.25wt%/15 min/1 atm /340 °C Desorption equilibrium pressure (340 °C): 9.0 atm Des temperature: 251 °C $\Delta H_{abs} = -62.7$ kJ·mol^{-1}·H_2	[65]
$Mg_2Ni_{0.7}Zr_{0.3}$	300	2	Ar	20:1	Des: 3.25wt%/60 min/1 atm /340 °C Desorption equilibrium pressure (340 °C): 10.1 atm Des temperature: 248 °C $\Delta H_{abs} = -59.8$ kJ·mol^{-1}·H_2	[65]
Mg_2Ni	-	72	Ar	8:1	Abs: 3.6wt%/10 h/150 °C Des: 3.0wt%/10 h/150 °C Absorption equilibrium pressure (150 °C): 2 bar Desorption equilibrium pressure (150 °C): 0.5 bar	[67]
$Mg_2Ni_{0.9}Cu_{0.1}$	600	60	Ar	20:1	Abs: 2.5wt%/100 s/400 °C	[68]
$Mg_2Ni_{0.7}Cu_{0.3}$	600	60	Ar	20:1	Abs: 2.3wt%/100 s/400 °C Desorption equilibrium pressure (400 °C): 0.13 MPa	[68]
$Mg_{1.95}Ti_{0.05}Ni_{0.8}Cr_{0.2}$	280	80	Ar	10:1	Abs: 3.12wt%/2 min/4.0 MPa/393 K	[70]
Mg–10wt%(1/4Y–3/4Ni)	225		Ar 2 h H_2 30 h	40:1	Des: 3wt%/300 °C	[77]

2.2. Modification Using Additives

2.2.1. Transition Metal Additives

At present, the added metal catalysts are mainly transition metals, in which V, Nb, Fe, Pd, Ni, Ti, Mn, Cr, etc. have been studied thoroughly [11,83–88].

The doping of V allows to significantly reduce the hydrogen desorption activation energy and increase the cycle stability of hydrogen absorption/desorption [85,89]. Liang et al. [86], using the ball milling method, produced nanocomposites MgH_2-5%Tm (molar percentage) (Tm = Ti, V, Mn, Fe, Ni) and conducted the systematic study of their hydrogen absorption/desorption properties. The results showed that these five transition metals catalyzed well the hydrogen absorption/desorption processes in MgH_2, and, in addition, the obtained nanocomposites were better in all properties than the pure ball milled MgH_2. In the range of 30~200 °C with respect to hydrogen absorption properties, the addition of Ti provided the fastest hydrogen absorption rate, and then V, Fe, Mn, and Ni, while with respect to hydrogen desorption properties, the most effective hydrogen desorption reaction was obtained by adding V, and then Ti, Fe, Ni and Mn. In the range of 250~300 °C the MgH_2-Ti composite best improves the kinetics of hydrogen desorption, while at temperatures below 250 °C MgH_2-V has the best kinetics of hydrogen desorption, even at 200 °C, 0.015 MPa can desorb hydrogen. Further studies of Liang et al. [90] showed that the good hydrogen desorption properties in MgH_2-5%V are due to the catalytic effect of vanadium and the powder of small-size vanadium particles and are also associated with the formation of the α-Mg nucleus on the $VH_{0.81}/MgH_2$ phase interfaces as a result of the strong affinity interaction between the vanadium and hydrogen atoms.

During ball milling and hydrogen absorption/desorption in Mg-based alloys the added transition metals sometimes form new metal hydrides, which can provide hydrogen diffusion channels, thereby improving hydrogen absorption/desorption kinetics. With ball milling MgH_2-5%Nb (molar percentage) for 20 h, followed by dehydrogenation, a metastable new phase $NbH_{0.6}$ was formed. This phase was

finally decomposed into Nb metal after approximately 200 s. This metastable new phase of Nb-hydride can be considered as an ordered structure with hydrogen vacancies that provide channels for the flow of hydrogen during the dehydrogenation of nanocomposites [91–93]. De Castro et al. [94] found that the NbH_2 new phase appeared in the MgH_2-5%Nb (molar fraction) nanocomposite prepared by ball milling under hydrogen atmosphere, while under the same preparation conditions in the ball-milled pure Nb. NbH_2 phase was not observed. This indicates that magnesium contributes to the hydrogenation of Nb, and Nb also contributes to the hydrogenation of magnesium. De Castro et al. attributed this synergistic behavior to the kinetic catalytic effects of the Mg/Nb nanointerface. In addition, the new phases produced during the ball milling process can also inhibit the reaggregation of powder particles during hydrogen absorption/desorption cycles [95].

Some of the doped metal catalysts can function as "hydrogen pumps" during hydrogen desorption. Janot et al. [96] prepared MgNi + 5wt%Pd using ball milling. It was found that after Pd was added, MgNi alloys began to desorb hydrogen at 150 °C, while the hydrogen desorption capacity increased to 1.5% (mass percent). This is mainly due to the catalytic effect of Pd, which acts as a "hydrogen pump" and accelerates the migration and diffusion of hydrogen across grain boundaries, transporting hydrogen from the inside of the alloy to the surface of the alloy.

The particle size of the doped metal catalysts also significantly influences the catalytic effects. Lee et al. [97] found that different sizes of Co particles had different catalytic effects on MgH_2. The researchers compared the catalytic effects of Co particles with sizes of 0.5~1.5 microns, 3~7 microns and 44 microns and concluded that with the size of 0.5~1.5 microns the catalytic effect was the best, whereas with the size of 3~7 microns it was the worst.

The lattice type of the alloy also affects its hydrogen storage properties. Luo et al. [98] using ball milling prepared Mg_xTi_{100-x} (x = 35, 50, 65, 80) alloys. It was observed that ball milled $Mg_{35}Ti_{65}$ alloy with BCC structure had 3.8% hydrogen storage capacity at 8 MPa hydrogen pressure and 200 °C, and showed good hydrogen absorption kinetics, while ball milled Mg_xTi_{100-x} (x = 50, 65, 80) alloys with FCC phase or HCP (main phase) + FCC mixed phases had a smaller hydrogen storage capacity, which was less than 1.2%.

Details of the investigation results of the part of the above selected works on modification using transition metal additives are presented in Table 2.

Table 2. Hydrogen storage properties of selected Mg modified by transition metal additives.

Material	Rotation Speed, rpm	Time, h	Atmosphere	Ball-to-Powder Weight Ratio	Hydrogen Storage Properties	Ref.
Mg–10.7wt%Ti–10.9wt%Al–0.7wt%Zr–0.1wt%C	400	12	Ar	60:1	Abs: 4.17wt%/10 min/1.5 MPa/573 K Des: 4.7wt%/20 min/0.0005 MPa/573 K ΔH_{des} = 74.9 kJ·mol^{-1}·H_2 ΔS_{des} = 136.6 J mol^{-1}·K^{-1} H_2 ΔH_{des} = 75.9 kJ·mol^{-1}·H_2 ΔS_{des} = 137.5 J mol^{-1}·K^{-1} H_2	[11]
MgH_2–5wt%TiH_2	320	30	-	50:1	Abs: 5.8wt%/2.5 min /15 atm/300 °C Des: 5.9wt%/20 min/1 atm/300 °C Full Des: 6.0wt%/374 °C Des temperature: 260 °C	[83]
MgH_2	320	30	-	50:1	Abs: 1.7wt%/2.5 min/15 atm/300 °C Des: 0.6wt%/20 min/1 atm/300 °C Full Des: 6.70wt%/410 °C Des temperature: 354 °C	[83]
MgH_2–Fe	650	2	Ar	-	Des temperature: 256.4 °C	[87]
Mg–5wt%Ni–2.5wt%Fe–2.5wt%Ti	250	4	H_2 (12 bar)	45:1	Abs: 4.0wt%/10 min/12 bar/300 °C Des: 4.2wt%/60 min/1.0 bar/300 °C	[89]
Mg–5wt%Ni–2.5wt%Fe–2.5wt%Ti	250	8	H_2 (12 bar)	45:1	Abs: 4.7wt%/10 min/12 bar/300 °C Des: 1.5wt%/60 min/1.0 bar/300 °C	[89]

Table 2. *Cont.*

Material	Rotation Speed, rpm	Time, h	Atmosphere	Ball-to-Powder Weight Ratio	Hydrogen Storage Properties	Ref.
$Mg_{92}In_5Zn_3$	300	80	Ar	30:1	Abs: 3.5wt%/1800 s/1.0 MPa/573 K ΔH_{des} = −68.6 kJ·mol^{-1}·H_2 ΔS_{des} = 134.5 J mol^{-1}·K^{-1} H_2 *Ea* (abs) = −62.5 kJ·mol^{-1}·H_2	[95]
Mg–10wt%Co(0.5–1.5 μm)	200	2	H_2 (11 bar)	9:1	Abs: 1.3wt%/60 min/11.2 bar/598 K	[97]
Mg–10wt%Co(3–7 μm)	200	2	H_2 (11 bar)	9:1	Abs: 0.3wt%/60 min/11.2 bar/598 K	[97]
Mg–10wt%Co(44 μm)	200	2	H_2 (11 bar)	9:1	Abs: 0.7wt%/60 min/11.2 bar/598 K	[97]

2.2.2. Metal Oxide Additives

Metal oxides, as a catalyst, on the one hand, can play the role of hydrogen absorption/desorption catalyzing, on the other hand, since the oxide is brittle, they can play the role of grinding aid refining particles during ball milling which helps to form nanomaterials. The reason for improved kinetics by doping transition metal oxides lies in the following: transition metal oxides are sensitive to hydrogen molecules thus even at lower temperatures a large amount of hydrogen molecules can be adsorbed on the surface, so that the hydrogen molecules are in an activated state and the bond energy between the hydrogen atoms is weakened, which makes the hydrogen molecules be decomposed easier into hydrogen atoms. Since the catalysis is usually bidirectional, the addition of a transition metal oxide is also advantageous for hydrogen desorption [99–107].

Widely used metal oxide catalysts are V_2O_5, TiO_2, Fe_2O_3, Fe_3O_4, Cr_2O_3, Al_2O_3, MnO_2, Nb_2O_5 etc. [101,102,108–115]. Oelerieh et al. [108,116] added Sc_2O_3, TiO_2, V_2O_5, Cr_2O_3, Mn_2O_3, Fe_3O_4, CuO, Al_2O_3 and SiO_2 respectively to compare their catalytic effects on the hydrogen absorption/desorption properties of MgH_2. The results showed that metal oxides with single valence (Sc_2O_3, Al_2O_3, SiO_2) had little effect on hydrogen absorption/desorption properties of MgH_2, while metal oxides with variable valence (TiO_2, V_2O_5, Cr_2O_3, Mn_2O_3 and Fe_3O_4) had excellent catalytic effect. This is due to the fact that oxides of polyvalent metals allow increase the probability of electron exchange reaction between oxides and hydrogen molecules so that the gas-solid reaction is accelerated. Doping metal oxides with variable valence also allows improve the hydrogen absorption/desorption cycle stability of the alloy [111,117]

V_2O_5 has a good catalytic effect. It can faster chemically adsorb hydrogen molecules on its surface. This adsorption effect can even directly decompose hydrogen molecules into hydrogen atoms, which can make hydrogen atoms enter the metal lattice faster, thereby greatly accelerating the hydrogen absorption process. For instance, nanocrystalline composites Mg-Ni-V_2O_5 can adsorb hydrogen up to more than 6.2% (mass percent) at 200 °C in 60 s; at 300 °C, 0.1 MPa can desorb hydrogen up to 6.0% (mass percent) in 700 s. doping V_2O_5 not only improves hydrogen absorption/desorption rate, but also decreases the hydrogen desorption temperature by about 30 °C [118].

For multivalent metal oxide catalysts, the hydrogen absorption/desorption cycles are usually accompanied by oxidation/reduction of the oxide. For example, for nanocrystalline composites Mg-3Ni-2Cr_2O_3 it is believed that the two-position mechanism where two Cr^{3+} function as an activation center for hydrogen absorption/desorption may serve as the catalytic mechanism of Cr_2O_3 [119]. According to the crystal field theory, the d^3 configuration of Cr^{3+} ions in Cr_2O_3 is the high-spin octahedral configuration. Under the effect of hydrogen molecules or hydrogen atoms Cr^{3+} in Cr_2O_3 can be reduced to Cr^{2+}, obtaining an electron from a hydrogen atom. Due to the fact that in a high-spin octahedral field, the stabilization energy of the d^3 configuration of Cr^{2+} ions is less than that of the d^3 configuration of the Cr^{3+} ions (i.e., the stability of Cr^{3+} is greater than the stability of Cr^{2+}), an unstable state is formed. Cr^{2+} ion again loses the electron and turns from an unstable state into Cr^{3+}. At the same time H^+ turns to hydrogen atom, obtaining an electron from Cr^{2+} ion. Thus, the kinetic balance is built. Similar results have been observed by Song et al. [120]. Song et al. has also found that the addition of an oxide catalyst such as Cr_2O_3 contributes to the refinement of the Mg powder during the ball milling process.

Barkhordarian et al. [112,121] investigated and compared the average hydrogen desorption rate of MgH_2 from 20% to 80% of the maximum hydrogen storage capacity using various metal oxide catalysts and concluded that Nb_2O_5 is the most catalytically active transition metal oxide. Figure 1 showed the hydrogen desorption rate of MgH_2 with different doped metal oxides at 573K in a vacuum state. Using the kinetic rate constants at 300 °C and 250 °C. Barkhordarian et al. reported that the desorption activation energy varies exponentially with Nb_2O_5 concentration and reaches the limit of 61 kJ/mol at 1 mol%. Further, the researchers also presumed that much poorer catalytic effect of the pure metals than that of the respective oxide is possibly due to pure metal itself not having the catalytic effect, as most pure metals exhibit the catalytic effect because there are oxides in the samples. However, this kind of explanation has not been confirmed, as in order to study the catalytic effect, the samples are not to be exposed to ambient air at any time. Oliver et al. [122] investigated hydrogen absorption mechanism of MgH_2/Nb_2O_5 and using the channel model interpreted the reason why Nb_2O_5 can greatly improve the hydrogen desorption kinetics of magnesium. In the first hydrogen desorption process, a redox reaction occurs between Nb_2O_5 and magnesium. The resulting magnesium–niobium oxide is dispersed in the sample and appears on the surface of the sample. Since Nb has different valence states, binary magnesium–niobium oxide channels having different stoichiometry are formed. These channels are distributed in the sample to facilitate the diffusion of hydrogen and enhance hydrogen desorption kinetics of the sample.

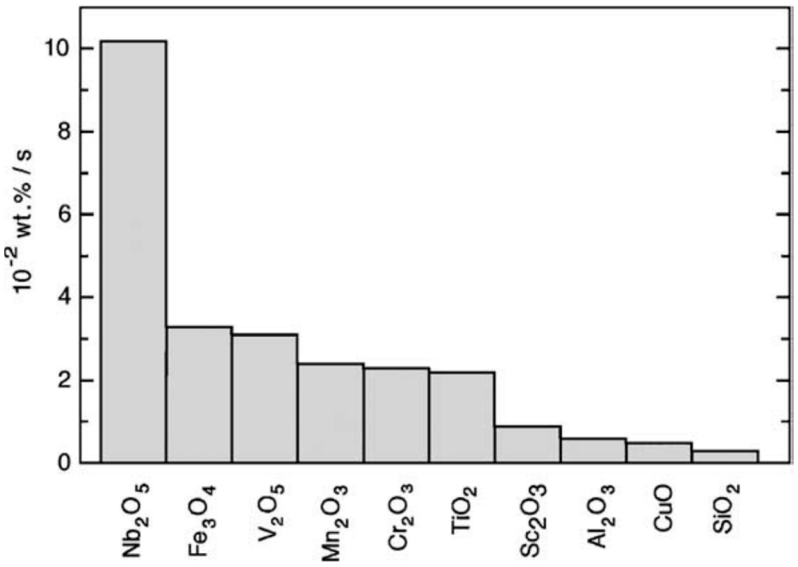

Figure 1. Comparison of the desorption rates of MgH_2 with different metal oxide catalyst additions at 300 °C into vacuum [112].

Details of the investigation results of the part of the above selected works on modification using metal oxide additives are presented in Table 3.

Table 3. Hydrogen storage properties of selected Mg modified by metal oxide additives.

Material	Rotation Speed, rpm	Time, h	Atmosphere	Ball-to-Powder Weight Ratio	Hydrogen Storage Properties	Ref.
MgH_2–4wt%Ni	400	10	H_2 (10 bar)	40:1	Des: 7.0wt%/300 °C Des temperature: 264 °C	[101]
MgH_2–6wt%TiO_2	400	10	H_2 (10 bar)	40:1	Des: 5.6wt%/350 °C Des temperature: 308 °C	[101]
MgH_2–4wt%Ni–6wt%TiO_2	400	10	H_2 (10 bar)	40:1	Des: 6.0wt%/300 °C Des temperature: 259 °C	[101]
MgH_2–10wt%Ni/TiO_2 (Ni/TiO_2 is nanocomposite with a mass ratio of 4:6)	400	10	H_2 (10 bar)	40:1	Des: 6.5wt%/300 °C Des temperature: 231 °C	[101]

Table 3. *Cont.*

Material	Rotation Speed, rpm	Time, h	Atmosphere	Ball-to-Powder Weight Ratio	Hydrogen Storage Properties	Ref.
MgH_2–8wt%Nb_2O_5–2wt%Ni	200	50	H_2 (10 bar)	34:1	Des: 5.5wt%/7 min/0.2 bar/225 °C ΔH_{abs} = 72.74 kJ·mol^{-1}·H_2	[105]
$(MgH_2)_{84}(TiH_2)_{10}(TiO_2)_6$	-	4	Ar	10:1	Abs: 5wt%/60 s/20 atm/300 °C Des: 4.8wt%/1250 s/0.2 atm/300 °C E_a(des) = 118 kJ·mol^{-1}·H_2	[106]
MgH_2–17wt%Nb_2O_5	-	20	Ar	-	Abs: 6wt%/400 s/1 MPa/300 °C Des: 6wt%/1000 s/0.1 kPa/300 °C Des temperature: 300 °C	[107]
MgH_2–17wt%Nb_2O_5	-	200	Ar	-	Abs: 6wt%/100 s/1 MPa/300 °C Des: 6wt%/250s/0.1 kPa/300 °C Des temperature: 264 °C	[107]
MgH_2–5mol%CuO	-	100	Ar	10:1	Abs: 5.5wt%/90 s/8.4 bar/300 °C	[108]
MgH_2–5mol%Mn_2O_3	-	100	Ar	10:1	Abs: 4.8wt%/90 s/8.4 bar/300 °C	[108]
MgH_2–5mol%Cr_2O_3	-	100	Ar	10:1	Abs: 4.5wt%/90 s/8.4 bar/300 °C	[108]
MgH_2–5mol%Fe_3O_4	-	100	Ar	10:1	Abs: 4.2wt%/60 s/8.4 bar/300 °C	[108]
MgH_2–5mol%V_2O_5	-	100	Ar	10:1	Abs: 4wt%/60 s/8.4 bar/300 °C	[108]
Mg–20wt%TiO_2	-	-	H_2 (0.8 MPa)	20:1	Abs: 3.7wt%/10 min/2.0 MPa/200 °C	[109]
Mg–10wt%Fe_2O_3	250	24	H_2 (10 bar)	9:1	Abs: 5wt%/60 min/12 bar/593 K	[110]
Mg–10wt%Fe_2O_3	250	8	H_2 (10 bar)	9:1	Abs: 3.3wt%/60 min/12 bar/593 K	[110]
Mg–10wt%Fe_2O_3	200	1	H_2 (10 bar)	9:1	not absorb hydrogen	[110]
Mg–10wt%Al_2O_3	-	2	H_2	9:1	Abs: 5.4wt%/60 min/11 bar/573 K	[120]
Mg–10wt%CeO_2	-	2	H_2	9:1	Abs: 3.2wt%/60 min/11 bar/573 K	[120]

2.2.3. Transition Metal Halide Additives

Many metal halides have a good catalytic effect on the hydrogen desorption temperature and hydrogen absorption kinetics of magnesium-based hydrogen storage materials [123–128]. Jin et al. [129,130] investigated the effect of transition metal fluorides on the hydrogen absorption/desorption properties of MgH_2. As shown in Figure 2, many fluorides had a positive catalytic effect on the hydrogen absorption kinetics of MgH_2. Among them, NbF_5 and TiF_3 significantly improved the hydrogen absorption kinetics of MgH_2. Jin et al. believed that the key to improving the hydrogen absorption kinetics of MgH_2 is the single-phase metal hydrides, formed in the reaction of MgH_2 with these transition metal fluorides during ball milling or hydrogen absorption. These unique single-phase metal hydrides are believed to effectively inhibit the growth of the MgH_2 nanoparticles during balling milling and hydrogen absorption/desorption cycles and there by maintaining a better catalytic activity in the hydrogen absorption/desorption cycles.

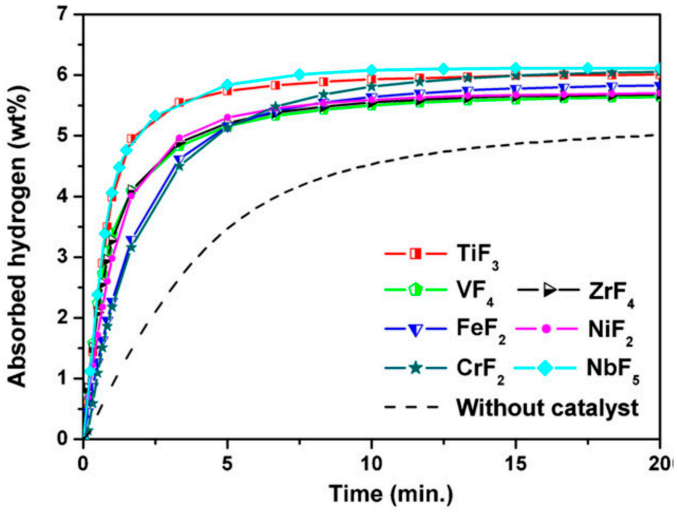

Figure 2. Hydrogenation kinetics of MgH_2 at 573 K under 10 bars of hydrogen with 1 mol% transition metal fluorides [129].

It should be noted that different amounts of additives NbF_5 and different ball milling times have different catalytic effects on the hydrogen absorption/desorption properties of MgH_2 [131]. Luo et al. [132] investigated the influence of different amounts of additives NbF_5 on catalytic effect. Results showed that when adding 2% (molar percentage) NbF_5, the most rapid kinetics was achieved. After ball milling of MgH_2 + 2%NbF_5 (molar percentage) for 5 h, at 300 °C 5 mass% absorption was achieved within 12 min and 6 mass% absorption was achieved within 60 min. The addition of NbF_5 leaded to decrease in the hydrogen desorption temperature by 64 °C and the hydrogen desorption activation energy was reduced to 90 kJ/mol, decreasing by 30 kJ/mol compared to pure MgH_2. Recham et al. [133] also believed that 2% NbF_5 (molar percentage) is the best doping amount, which leads to significant reduction in hydrogen desorption temperature of MgH_2.

It is worth noting that the anion species of the halides have a great influence on their catalytic effects: usually the catalytic effect of chloride is worse than that of fluoride. Malka et al. [134] compared the influence of different chlorides and fluorides on the decomposition temperature of MgH_2 as measured by temperature programmed desorption (TPD). As shown in Figure 3, the fluorides, as compared to the chlorides, had much stronger influence on the MgH_2 decomposition process. In all chlorides only $TiCl_3$ lead to the reduction of the desorption temperature down to below 300 °C. In the case of the fluorides ZrF_4, NbF_5, TaF_5, TiF_3 and FeF_2 a strong catalytic influence on MgH_2 decomposition was exhibited. The largest reduction of hydrogen desorption temperature was observed for the ZrF_4 additive, which allowed hydrogen desorption start below 250 °C. This data is in agreement with the results presented by Jin et al. [129], de Castro et al. [135] and Deledda et al. [136]. The fact that fluorides can significantly influence the desorption properties of MgH_2 may be caused by the presence of the F anions, which weaken the Mg–H bonding and led to the formation of MgF_2, providing electron-rich centers to trap the transition metal atoms. In addition, the F anion may tailor the electronic structure of the transition metal atom to influence its activity for hydrogen dissociation/recombination. The ZrF_4 additive exhibits a different mechanism and is unchanged after milling and desorption/absorption cycle. It is possible that the catalytic function of ZrF_4 is due to the presence of both Zr atoms and F anions in the sample that facilitated the recombination of H_2 molecules on the surface of ZrF_4 [137,138].

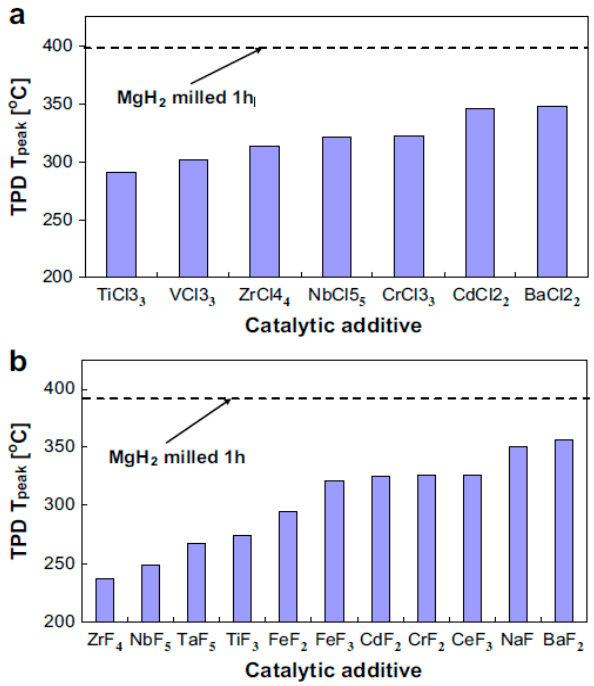

Figure 3. Maximum temperature of MgH_2 decomposition TPD. peak (T peak) catalyzed by 7 wt% of various halide additives:(**a**) chlorides and (**b**) fluorides [134].

There are also studies showing that mechanical alloying of halides and alloys of Mg or Mg–Ni both reduces the size of the metal powder and modifies the surface of metals (destroy the oxide layer on the metal surface), thereby stimulating the hydrogen absorption/desorption, in particular, stimulating the first hydrogen absorption/desorption [139].

Details of the investigation results of the part of the above selected works on modification using transition metal halide additives are presented in Table 4.

Table 4. Hydrogen storage properties of selected Mg modified by transition metal halide additives.

Material	Rotation Speed, rpm	Time, h	Atmosphere	Ball-to-Powder Weight Ratio	Hydrogen Storage Properties	Ref.
Mg–15wt%TiF_4	400	2	Ar (0.1 MPa)	20:1	Des temperature: 150 °C *Ea* (des) = 77 kJ·mol^{-1}·H_2	[123]
MgH_2–0.4mol%$NbCl_5$	-	2	Ar	-	Des:5.2wt%/50 min/primary vacuum/300 °C	[124]
MgH_2–0.4mol%CaF_2	-	2	Ar	-	Des:5.8wt%/50 min/primary vacuum/300 °C	[124]
MgH_2–5wt%K_2NbF_7	400	3	Ar	80:1	Abs: 5.7wt%/2.3 min/27 atm/320 °C Des: 5.7wt%/4.6 min/1 atm/320 °C Full Des: 6.5wt%/350 °C Des temperature: 255 °C	[125]
MgH_2 as milled	400	3	Ar	80:1	Abs: 7.0wt%/6.5 min/27 atm/320 °C Des: 0.2wt%/4.6 min/1 atm/320 °C Full Des: 6.8wt%/450 °C Des temperature: 330 °C	[125]
Pristine MgH_2	-	-	-	-	Des: Full Des: 7.0wt%/425 °C Des temperature: 414 °C	[125]
MgH_2–10wt%FeF_3	400	15	H_2 (1 MPa)	40:1	Abs: 4.03wt%/5 min/3.5 MPa/473 K Des: 5.92wt%/8 min/0.01 MPa/573 K *Ea* (des) = 77.6 kJ·mol^{-1}·H_2	[127]
MgH_2–10wt%TiF_3	-	-	-	-	Abs: 4.2wt%/5 min/3.5 MPa/473 K Des: 6.04wt%/8 min/0.01 MPa/573 K *Ea* (des) = 74.1 kJ·mol^{-1}·H_2	[127]
MgH_2–0.2mol% NbF_5	-	25	Ar	16:1	Des: 5.6wt%/25 min/10^{-1} mbar/300 °C	[133]
MgH_2–2mol% NbF_5	-	25	Ar	16:1	Des: 5.8wt%/25 min/10^{-1} mbar/300 °C *Ea* (des) = 88 kJ·mol^{-1}·H_2	[133]
MgH_2–2mol%NbF_5	-	1	Ar	16:1	Des: 4.4wt%/40 min/10^{-1} mbar/250 °C *Ea* (des) = 72 kJ·mol^{-1}·H_2	[133]
MgH_2–7wt%$TiCl_3$	650	1	Ar	25:1	Abs: 6.4wt%/1.9 min/10 bar/325 °C Des: 6.1wt%/4 min/1 bar/325 °C	[137]
MgH_2–7wt%ZrF_4	650	1	Ar	25:1	Abs: 6.4wt%/2.0 min/10 bar/325 °C Des: 6.3wt%/1.6 min/1 bar/325 °C	[137]

2.2.4. Carbon Additives

Carbon materials have high specific surface area, can store hydrogen at low temperatures and are low costing. Hence magnesium-carbon nanocomposites attract the attention of many scientists. Currently, the widely studied carbon materials that are part of the magnesium-carbon composites include graphite, carbon nanotubes, carbon, graphene, activated carbon, microlitic carbon, etc. [140–148].

Yu et al. [149] prepared Mg–3Ni–2MnO_2–0.25CNTs using mechanical ball milling. The results showed that hydrogen capacity of this material reached 7.0%, the hydrogen absorption reaction was quickly completed within 100 s, the hydrogen desorption reaction was completed within 600 s at 0.1 MPa, and the temperature of the hydrogen desorption platform was approximately 280 °C. Yu et al. considered that the excellent hydrogen storage properties of the CNTs-doped alloy are related to the strong adsorption ability of carbon nanotubes for hydrogen molecules and the excellent heat transfer performance of carbon nanotubes.

It is believed that there is the synergistic effect between ball milling and carbon material. On the one hand ball milling can shorten the length of carbon nanotubes, open the tube port, increase the surface area, and increase the hydrogen adsorption capacity of carbon nanotubes [150] On the other hand, with increase of absorbed carbon component on freshly exposed Mg surfaces, the impermeable

surface oxide/hydroxide layer is not reformed and the composite is readily accessible to hydrogen, which enhances the ball milling effect [151]. The inhibition effect of carbon materials on reformed oxides can be explained by two different mechanisms: one is that in the initial stage of the milling process, a stack of carbon layers is adsorbed on freshly created Mg surfaces, which lower the surface tension of the compound, thereby reducing the driving force responsible for the diffusion of oxygen atoms to the surface, therefore to certain extent altering the formation of the impermeable surface oxide layer. Besides, the breaking of C–C bonds in the carbon layer and the presence of radicals yield to the formation of highly reactive C species which might be oxidizing enough to react with oxygen-containing species that are either present at the surface of Mg or diffuse to the surface [152]. It is worth noting that unhybridized electrons of carbon fragments produced from the ball-milling process can not only absorb oxygen-containing species, but also interact with hydrogen molecules, which increases the hydrogen diffusion driving force [153–155].

Zhou et al. [156,157] found that microlitic carbon has a graphite-like crystal structure, and like graphite and graphene, has a good grinding effect on magnesium, the former can prevent the powder from agglomerating, and can quickly refine the magnesium particles. The particle size of magnesium powder ball milled for 2 h was down to 30–50 nm when doped by 40% microlitic carbon. In addition, it was found that between microlitic carbon and magnesium there is a synergistic effect on hydrogen storage. This synergistic effect is concluded in the following two aspects: (1) Under the action of magnesium, hydrogen molecules decompose into hydrogen atoms, which can either form ≡CH, $=CH_2$, $–CH_3$ as a result of combination of hydrogen atoms with broken bonds on the surface of carbon particles (chemical absorption), or enter into the space between carbon microcrystalline layers, thereby hydrogen is stored in carbon (physical absorption); (2) Microlitic carbon can significantly reduce hydrogen desorption temperature of MgH_2. This is due to the function of microlitic carbon as a grinding aid, which allows reduce the size of magnesium grains, increase the specific surface, increase structural defects and increase the activity of dehydrogenation. Unlike Zhou et al., based on crystal structure characteristics of microlitic carbon and magnesium Lu and Tang [158] explained the synergistic effect between microlitic carbon and magnesium: (1) The disordered structure of long chains in combination with the ordered structure of short chains in microscopic carbon determines their good grindability, greater brittleness, good dispersion and lubricity, which facilitates pulverize and disperse magnesium particles during ball milling, thereby fastening nanocrystallization; (2) Mutual peritectics are formed between the atoms of carbon and magnesium, which on the one hand, provides for the catalyst with carriers, so that the catalyst can be distributed more homogeneously in the hydrogen storage material, and on the other hand, provides the channels for the diffusion of hydrogen atoms.

Zhang et al. [159] studied the effect of carbon material doping on the hydrogen desorption properties of MgH_2 and its microscopic mechanism according to the first principle. The calculations showed that the intrinsic reason for the improved hydrogen desorption properties of MgH_2 by the carbon material doping is that its doping reduces the dissociation energy of H atoms from the MgH_2 matrix, weakening the bond strength of Mg–H.

Wu et al. compared the effect of single CNTs, the single metal catalyst and combination of CNTs and metal catalyst on hydrogen storage properties of MgH_2 [160–163]. They found that CNTs allowed to significantly increase hydrogen storage capacity, however, it was not as good as a metal catalyst in terms of increasing the hydrogen absorption/desorption rate. In addition, it was found that the synergistic effect of the metal catalyst and carbon enabled higher hydrogen storage capacity and faster hydrogen absorption rate. Research of Li et al. proved this point [164]. The co-catalytic effect for hydrogenation may be understood as a spillover mechanism through the interaction of facile p-electrons of carbon with metallic catalyst [165].

Details of the investigation results of the part of the above selected works on modification using carbon additives are presented in Table 5.

Table 5. Hydrogen storage properties of selected Mg modified by carbon additives.

Material	Rotation Speed, rpm	Time, h	Atmosphere	Ball-to-Powder Weight Ratio	Hydrogen Storage Properties	Ref.
MgH_2	-	20	H_2 (10 bar)	21:1	Abs: 6.3wt%/35 min/50 bar/503 K	[142]
MgH_2–10wt%C_{60}	600	10	H_2 (10 bar)	21:1	Abs: 5.3wt%/35 min/50 bar/503 K	[142]
MgH_2–10wt%C_{60}	600	20	H_2 (10 bar)	21:1	Abs: 5.0wt%/35 min/50 bar/503 K	[142]
MgH_2–10wt%C_{60}	600	0.5	H_2 (10 bar)	21:1	Abs: 5.0wt%/35 min/50 bar/503 K	[142]
Mg–2wt%graphite	800	0.5	-	20:1	Abs: 6.0wt%/12.5 min Des:5.0wt%/200 min	[144]
Mg–2wt%graphite	800	4	-	20:1	Abs: 6.0wt%/12.5 min Des: 4.5wt%/200 min	[144]
Mg–2wt%graphite	800	38	-	20:1	Abs: 5.0wt%/12.5 min Des: 5.0wt%/200 min	[144]
Mg–2wt%MWCNTs	800	0.5	-	20:1	Abs: 6.5wt%/10 min Des: 6.5wt%/200 min	[144]
Mg–2wt%MWCNTs	800	4	-	20:1	Abs: 6.0wt%/12.5 min Des: 6.0wt%/200 min	[144]
Mg–2wt%MWCNTs	800	38	-	20:1	Abs: 5.0wt%/12.5 min Des: 2.8wt%/200 min	[144]
MgH_2–25at%CB (carbon black)	-	10	Ar	12:1	Abs: 7.0wt%/90 min/25 bar/300 °C	[147]
MgH_2–1mol%C_{60}	600	2	H_2 (10 bar)	21:1	Abs: 3.1wt%/20 min/400 °C Des temperature: 325 °C	[148]
MgH_2–1mol%C_{60}	600	2	Ar (1 bar)	21:1	Abs: 5.1wt%/20 min/400 °C Des temperature: 325 °C	[148]
Mg–5wt%MWNTs	-	3	H_2 (0.1 MPa)	20:1	Abs: 4.3wt%/15 min/2.0 MPa/373 K Abs: 4.9wt%/1 min/2.0 MPa/553 K	[151]
MgH_2–5wt%SWNTs	-	10	Ar	40:1	Abs: 5.3wt%/180 min/2.0 MPa/423 K Abs: 6.7wt%/2 min/2.0 MPa/573 K	[153]
MgH_2–5wt%BNNT (boron nitride nanotubes)	-	10	Ar	40:1	Abs: 1.3wt%/180 min/2.0 MPa/423 K Abs: 5.4wt%/10 min/2.0 MPa/573 K	[153]
MgH_2–5wt%AC (activated carbon)	-	10	Ar	40:1	Abs: 3.7wt%/180 min/2.0 MPa/423 K Abs: 5.8wt%/2 min/2.0 MPa/573 K	[153]

2.2.5. Intermetallic Compounds

Intermetallic compounds, widely used for alloying with magnesium-based materials, include La-Ni series compounds, Ti intermetallic catalysts, Mg-Ni series compounds etc. The general features of these composite materials are high hydrogen absorption/desorption capacity, low hydrogen desorption temperature [166–176].

Li et al. [175,176] investigated the influence of various La–Ni intermetallic catalysts on hydrogenation behavior of Mg-based alloys. The results showed that Mg–60%$LaNi_5$ had relatively high activity, so that 2.37 mass% absorption was achieved within 15 min at the room temperature, and at 553 K, the maximum hydrogen absorption capacity was 4.23 mass%. For Mg–30%$LaNi_{2.28}$ the maximum hydrogen absorption capacity at 553 K was 5.4 mass%. Liang et al. [177] found that the ternary Mg–Ni–La alloy exhibited much better absorption/desorption kinetics than that of the binary alloys Mg–La and Mg–Ni, besides, lanthanum hydride had strong catalytic effect on hydrogen absorption of Mg, but weak effect on hydrogen desorption. Similar results have been observed by the other research group [178].

Zhou et al. [179,180] investigated the effect of various Ti, V intermetallic catalysts on hydrogen storage properties of magnesium hydride. As shown in Figures 4 and 5, $TiMn_2$ doped MgH_2 had the lowest hydrogen desorption temperature and exhibited drastically improved hydrogen absorption kinetics at the room temperature. As shown in Figure 6, $V_{75}Ti_5Cr_{20}$ provided the largest hydrogen storage capacity at the room temperature, which was comparable to $TiMn_2$ doped MgH_2.

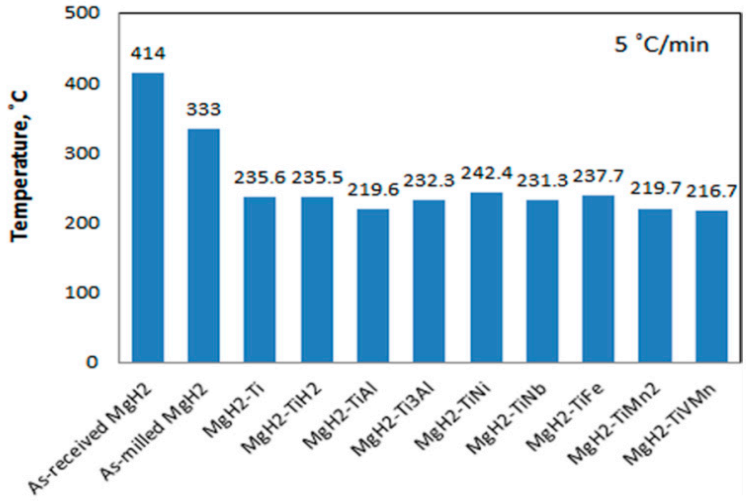

Figure 4. Dehydrogenation temperature of different Ti-based catalysts doped systems, determined by thermal gravimetric analyzer (TGA) profiles at fractional conversion $\alpha = 0.4$ [179].

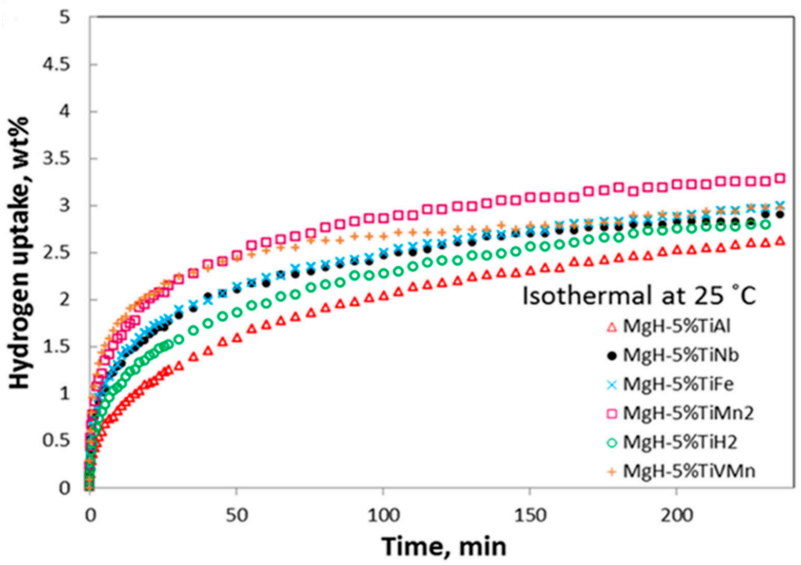

Figure 5. Effect of Ti-based catalysts on hydrogenation kinetics under hydrogen pressure of 1 bar [179].

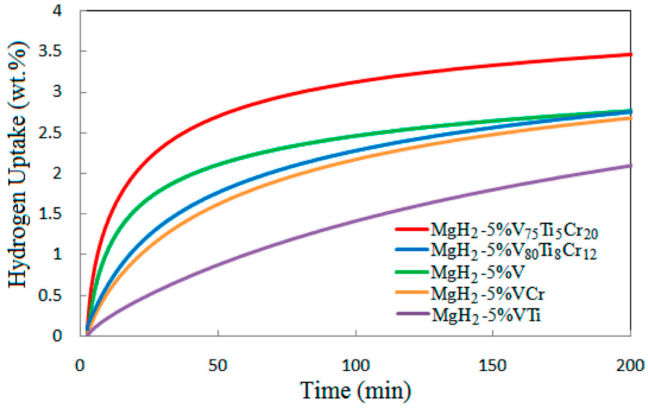

Figure 6. PCT (Pressure-Composition-Temperature) hydrogenation kinetics of MgH_2 with $V_{75}Ti_5Cr_{20}$, $V_{80}Ti_8Cr_{12}$, V, VCr, and VTi additives at the room temperature and 1 bar hydrogen pressure [180].

Another fast-developing intermetallic compound is the Zr-based alloy. 10% ZrNi-MgH_2 (mass fraction) completed 5% hydrogen absorption at 300 °C within 3 min and it took only 7 min to release the same amount of hydrogen, which suggested the excellent catalytic effect of Zr-based intermetallic compounds [181]. Makihara et al. [182] reported that Mg-50wt%$ZrMn_2$ completed 2.6% hydrogen absorption at 275 °C, while maximum hydrogen capacity of Mg-50wt%$ZrFe_{1.4}Cr_{0.5}$ was 3.2% at 300 °C and hydrogen desorption was completed at 0.1 MPa within 15 min [183].

Wang et al. [184] prepared Mg_x/Mg_2Ni (x = 10%, 30%, 50%) composite alloys by mixing and ball milling of the powder of Mg_2Ni alloys and magnesium. In contrast to the fact that with separate ball milling of Mg_2Ni alloys Mg_2Ni are decomposed into Mg and Ni, these mixed powders do not form new phases during ball milling due to the effective inhibition of decomposition of the Mg_2Ni phase by adding magnesium powder.

The intermetallic alloys have even more pronounced catalytic effects. It is not clear at present time, however, why the intermetallic alloys would have more significant effects than their elemental counter parts. One observation is that these alloys form less stable hydrides than their corresponding elemental metals.

Details of the investigation results of the part of the above selected works on modification using intermetallic compound additives are presented in Table 6.

Table 6. Hydrogen storage properties of selected Mg modified by intermetallic compounds.

Material	Rotation Speed, rpm	Time, h	Atmosphere	Ball-to-Powder Weight Ratio	Hydrogen Storage Properties	Ref.
Mg–11.5wt%LiCl–12.49wt%CB	-	15	H_2 (6N)	60:1	Abs: 5.2wt%/5 h/2.0 MPa/2.5 MPa 623K, ΔH_{des} = 74.2 kJ·mol^{-1}·H_2	[167]
Mg–9.09wt%$V_{0.81}Fe_{0.19}$	500	5	H_2 (30 bar)	36.4:1	Abs: 4.8wt%/10 min/10 bar/250 °C, *Ea* (des) = 60 kJ·mol^{-1}·H_2	[168]
Mg–16.67wt%$V_{0.81}Fe_{0.19}$	500	5	H_2 (30 bar)	33.3:1	Abs: 3.8wt%/40 min/10 bar/25 °C, *Ea* (des) = 33 kJ·mol^{-1}·H_2	[168]
MgH_2–10wt%$TiVO_{3.5}$	500	24	H_2 (50 bar)	120:1	Des: 6.6wt%/60 min/0.001 Torr/300 °C	[169]
MgH_2–5wt%Zr_8Ni_{21}		20	Ar	10:1	Abs: 5.3wt%/16 s/10 bar/250 °C Des: 6.5wt%/300 s/0.1 bar/300 °C	[170]
MgH_2–10wt%$FeNiH_x$	175	10	H_2 (0.7 MPa)	50:1	Abs: 5.6wt%/25 bar/300 °C Des: 6.4wt%/1 atm/325 °C	[171]
Mg–15wt%$Mg_2Ni_{0.9}Co_{0.1}$	200	0.5	Ar	10:1	Abs: 5.5wt%/40 min/1 MPa/473 K Des: 5.3wt%/90 min/0.15 MPa/573 K	[172]
Mg–15wt%$Mg_2Ni_{0.9}Fe_{0.1}$	200	0.5	Ar	10:1	Abs: 5.3wt%/10 min/1 MPa/573 K Des: 5.8wt%/60 min/0.15 MPa/573 K	[173]
Mg–7wt%FeNb granule	-	10	Ar	10:1	Abs: 5.5wt%/100 s/2.0 MPa/350 °C Des: 6.4wt%/450 s/0.01 MPa/350 °C	[174]
Mg–30wt%$LaNi_{2.28}$	-	80	H_2 (3.0 MPa)	10:1	Abs: 5.35wt%/50 s/3.0 MPa/553 K	[176]
Mg–30wt%$LaNi_{2.28}$	-	40	H_2 (3.0 MPa)	10:1	Abs: 4.5wt%/420 s/3.0 MPa/553 K	[176]
MgH_2–30wt%$LaNi_5$	-	20	Ar	10:1	Abs: 4.5wt%/400 s/1.0 MPa/423 K Des: 4.6wt%/200 s/0.015 MPa/573 K	[177]
Mg–30wt%$LaNi_5$	-	20	Ar	10:1	Abs: 4.1wt%/1000 s/1.0 MPa/423 K Des: 5.0wt%/150 s/0.015 MPa/573 K	[177]
MgH_2–5wt%$LaNi_5$	300	40	H_2 (1 bar)	15:1	Abs: 5.5wt%/180 s/20 bar/245 °C Des: 3.6wt%/2 h/245 °C	[178]
MgH_2–5wt%$LaNi_5$	300	20	H_2 (1 bar)	15:1	Abs: 5.5wt%/1 h/20 bar/245 °C Des: 3.0wt%/2 h/245 °C	[178]

3. Summary

In this paper, different modification methods by ball milling were reviewed. It is clear that ball milling is the promising method for preparing hydrogen storage alloys, especially hydrogen storage alloys with amorphous and nanocrystalline structures, as it significantly improves their hydrogen storage properties, including kinetic properties, electrochemical properties and cycle stability. Ball milling has opened up new avenues for the field of synthetic magnesium-based hydrogen storage materials. However, ball milling still possesses certain limitations. For example, in hydrogen absorption/desorption cycles defects caused by ball milling will disappear, nanograin will agglomerate, and MgO will reform.

Adding catalysts such as transition metals, metal oxides, intermetallic compounds, transition metal halides, and carbon materials to magnesium-based hydrogen storage materials can not only improve the hydrogen absorption/desorption kinetics, but also appropriately reduce the hydrogen absorption/desorption temperature. Moreover, there is probability for the synergistic effect between catalysts and ball milling process, effectively improving the limitations of ball milling. The catalytic effects of different types of catalysts are quite different. In general, transition metal halides, multivalent transition metal oxides and carbon materials have better catalytic effects. These types of catalysts not only promote the refinement of the metal powder during ball milling, but also modify the metal as well as inhibit the reformation of MgO and the agglomeration of crystal grains in hydrogen absorption/desorption cycles, thus further improving the hydrogenation-dehydrogenation kinetics and the cycle stability. However, all current modification approaches only improve one or two aspect of hydrogen storage properties, the comprehensive properties have not been significantly improved, i.e., to date no single catalyst can significantly lower the hydrogen desorption temperature, increase the hydrogen absorption/desorption rate, or increase the cycle stability of hydrogen absorption/desorption while maintaining the high hydrogen storage capacity of pure magnesium. From this review it can be concluded that each type of additive has its own advantages and limitations. In general, carbon additives are recommended if an increase in hydrogen storage capacity is desired, while niobium-containing fluoride or oxide additives are recommended if the kinetics of hydrogen absorption/desorption (lowering the hydrogen absorption/desorption temperature, increasing the rate of hydrogen absorption/desorption) are to be well improved. Furthermore, the vanadium additive is a good choice for improving the stability of hydride absorption/desorption cycles. Characteristics of the different additives mentioned above should be taken into account when new materials are designed.

The action mechanism of various catalyst systems is still unclear, and many conclusions still differ. In view of the current research status and development trends, we believe that there are two key research directions in the future: (1) The research of the hydrogen storage mechanism of various magnesium-based hydrogen storage materials, especially magnesium-based alloy materials and magnesium-based composite materials. Through the calculation of materials based on atomic scale (computer design of materials), selecting the appropriate alloy composition and ball milling parameters (ball milling time, ball-to-powder weight ratio, Ball mill speed, etc.) will be an effective way to realize large-scale practical use of magnesium-based hydrogen storage materials; (2) Development of a more optimized catalytic system by combining different types of catalysts based on current catalytic systems.

Funding: This work was carried out within the framework of the Competitiveness Enhancement Program of National Research Tomsk Polytechnic University (VIU-OEF-66/2019).

Conflicts of Interest: The authors declare no conflict of interest.

References

1. Murashkina, T.L.; Syrtanov, M.S.; Laptev, R.S.; Stepanova, E.N.; Lider, A.M. Structure and defects evolution at temperature and activation treatments of the $TiCr_2$ intermetallic compound of Laves phase C36-type. *Int. J. Hydrogen Energy* **2019**, *44*, 10732–10743. [CrossRef]
2. Murashkina, T.L.; Syrtanov, M.S.; Laptev, R.S.; Lider, A.M. Cyclic stability of the C36-type $TiCr_2$ Laves phase synthesized in the abnormal glow discharge plasma under hydrogenation. *Int. J. Hydrogen Energy* **2019**, *44*, 6709–6719. [CrossRef]
3. Kudiiarov, V.N.; Syrtanov, M.S.; Bordulev, Y.S.; Babikhina, M.N.; Lider, A.M.; Gubin, V.E.; Murashkina, T.L. The hydrogen sorption and desorption behavior in spherical powder of pure titanium used for additive manufacturing. *Int. J. Hydrogen Energy* **2017**, *42*, 15283–15289. [CrossRef]
4. Kudiiarov, V.N.; Kashkarov, E.B.; Syrtanov, M.S.; Lider, A.M. Hydrogen sorption by Ni-coated titanium alloy VT1-0. *Int. J. Hydrogen Energy* **2017**, *42*, 10604–10610. [CrossRef]
5. Nikitina, L.; Laptev, R.; Abzaev, Y.; Lider, A.; Ivashutenko, A. Positron spectroscopy of nanodiamonds after hydrogen sorption. *Nanomaterials* **2018**, *8*, 36. [CrossRef] [PubMed]

6. Pollet, B.G.; Staffell, I.; Shang, J.L. Current status of hybrid, battery and fuel cell electric vehicles: From electrochemistry to market prospects. *Electrochim. Acta* **2012**, *84*, 235–249. [CrossRef]
7. Zadorozhnyy, V.; Berdonosova, E.; Gammer, C.; Eckert, J.; Zadorozhnyy, M.; Bazlov, A.; Zheleznyi, M.; Kaloshkin, S.; Klyamkin, S. Mechanochemical synthesis and hydrogenation behavior of $(TiFe)_{100-x}Ni_x$ alloys. *J. Alloy. Compd.* **2019**, *796*, 42–46. [CrossRef]
8. Hua, T.; Ahluwalia, R.; Eudy, L.; Singer, G.; Jermer, B.; Asselin-Miller, N.; Wessel, S.; Patterson, T.; Marcinkoski, J. Status of hydrogen fuel cell electric buses worldwide. *J. Power Sour.* **2014**, *269*, 975–993. [CrossRef]
9. Huang, L.J.; Wang, H.; Liu, J.W.; Zhang, C.; Ouyang, L.Z.; Zhu, M. Low temperature de/hydrogenation in the partially crystallized $Mg_{60}Ce_{10}Ni_{20}Cu_{10}$ metallic glasses induced by milling with process control agents. *J. Alloy. Compd.* **2019**, *792*, 835–843. [CrossRef]
10. Zhu, Q.-L.; Xu, Q. Liquid organic and inorganic chemical hydrides for high-capacity hydrogen storage. *Energy Environ. Sci.* **2015**, *8*, 478–512. [CrossRef]
11. Kral, L.; Cermak, J. Improvement of hydrogen storage properties of Mg by catalytic effect of Al-containing phases in Mg-Al-Ti-Zr-C powders. *Int. J. Hydrogen Energy* **2019**, *44*, 13561–13568. [CrossRef]
12. Wang, L.; Quadir, M.Z.; Aguey-Zinsou, K.-F. Direct and reversible hydrogen storage of lithium hydride (LiH) nanoconfined in high surface area graphite. *Int. J. Hydrogen Energy* **2016**, *41*, 18088–18094. [CrossRef]
13. Lai, Q.; Paskevicius, M.; Sheppard, D.A.; Buckley, C.E.; Thornton, A.W.; Hill, M.R.; Gu, Q.; Mao, J.; Huang, Z.; Liu, H.K.; et al. Hydrogen storage materials for mobile and stationary applications: Current state of the art. *Chemsuschem* **2015**, *8*, 2789–2825. [CrossRef] [PubMed]
14. Pukazhselvan, D.; Kumar, V.; Singh, S.K. High capacity hydrogen storage: Basic aspects, new developments and milestones. *Nano Energy* **2012**, *1*, 566–589. [CrossRef]
15. Nielsen, T.K.; Besenbacher, F.; Jensen, T.R. Nanoconfined hydrides for energy storage. *Nanoscale* **2011**, *3*, 2086. [CrossRef] [PubMed]
16. Zeng, X.; Ding, W.; Ying, Y.; Zou, J. Research progress of Mg-based energy materials. *Mater. Chin.* **2011**, *30*, 35–43. (In Chinese)
17. Cortez, J.J.; Castro, F.J.; Troiani, H.E.; Pighin, S.A.; Urretavizcaya, G. Kinetic improvement of H_2 absorption and desorption properties in Mg/MgH_2 by using niobium ethoxide as additive. *Int. J. Hydrogen Energy* **2019**, *44*, 11961–11969. [CrossRef]
18. Crivello, J.-C.; Dam, B.; Denys, R.V.; Dornheim, M.; Grant, D.M.; Huot, J.; Jensen, T.R.; de Jongh, P.; Latroche, M.; Milanese, C.; et al. Review of magnesium hydride-based materials:Development and optimisation. *Appl. Phys. A* **2016**, *122*, 97. [CrossRef]
19. Wang, L.; Wang, S.h.; Sun, C.h. Developments in the researches of Mg-based hydrogen storage materials (in Chinese). *J. Shijiazhuang Vocat. Technol. Inst.* **2016**, *28*, 50–53. [CrossRef]
20. Aguey-Zinsou, K.F.; Ares-Fernández, J.R. Hydrogen in magnesium: New perspectives toward functional stores. *Energy Environ. Sci.* **2010**, *3*, 526–543. [CrossRef]
21. Luo, X.; Zhang, J.; Jing, X.; Hu, B. The research status and development of hydrogen storage materials (in Chinese). *Mater. Rev.* **2007**, *21*, 118–120, 135.
22. Zhang, J.; Li, Z. Research Progress of preparation methods of Mg-based hydrogen storage Alloy. *Hot Work Technol.* **2014**, *43*, 7–9, 13. (In Chinese) [CrossRef]
23. Ma, X.; Yue, L.; He, G.; He, D.; Zhang, J. Research development of mechanical alloying used to synthesize Mg-based hydrogen storage alloys (in Chinse). *Mater. Rev.* **2010**, *24*, 89–92, 98.
24. Chen, J.; Shi, Y.; Zhang, F.; Han, Y. The mechanism of MA in high energy ball-milling technology. *Machinery* **2004**, *31*, 52–54. (In Chinese) [CrossRef]
25. Liu, Y.; Wang, J.; Zhang, M.; Qin, X. Research and development of mechanical attrition method in nanostructural materials. *Mater. Rev.* **2003**, *17*, 20–22, 29. (In Chinese) [CrossRef]
26. Zhao, D.L.; Zhang, Y.H. Research progress in Mg-based hydrogen storage alloys. *Rare Metals* **2014**, *33*, 499–510. [CrossRef]
27. Li, B.; Li, J.; Zhao, H.; Yu, X.; Shao, H. Mg-based metastable nano alloys for hydrogen storage. *Int. J. Hydrogen Energy* **2019**, *44*, 6007–6018. [CrossRef]
28. Shao, H.; Xin, G.; Zheng, J.; Li, X.; Akiba, E. Nanotechnology in Mg-based materials for hydrogen storage. *Nano Energy* **2012**, *1*, 590–601. [CrossRef]

29. Wang, Y.; Wang, Y. Recent advances in additive-enhanced magnesium hydride for hydrogen storage. *Prog. Nat. Sci. Mater. Int.* **2017**, *27*, 41–49. [CrossRef]
30. Bouaricha, S.; Dodelet, J.P.; Guay, D.; Huot, J.; Schulz, R. Activation characteristics of graphite modified hydrogen absorbing materials. *J. Alloy. Compd.* **2001**, *325*, 245–251. [CrossRef]
31. Xu, W.; Tao, Zh.; Chen, J. Progress of research on hydrogen storage. *Prog. Chem.* **2006**, *18*, 200–210. (In Chinese) [CrossRef]
32. Lin, J.; Zhao, D.; Wang, L. Hydrogen storage materials and research progress. *J. Suihua Univ.* **2017**, *37*, 141–145. (In Chinese)
33. Li, X.; Xu, H.; Cheng, P. The Review of hydrogen storage materials. *Hebei Chem. Ind.* **2012**, *35*, 51–53. (In Chinese) [CrossRef]
34. Zhang, Y.; Zhao, D.; Han, X.; Li, B.; Dong, X.; Wang, X. Electrochemical characteristics of mechanical alloyed $\left(Mg_{1-x}Zr_x\right)_2Ni$ (x = 0–0.1) electrode alloys. *Int. J. Hydrogen Energy* **2007**, *32*, 2830–2835. [CrossRef]
35. Yuan, H.; Li, Q.; Song, H.; Wang, Y.; Liu, J. Electrochemical characteristics of Mg_2Ni-type alloys prepared by mechanical alloying. *J. Alloy. Compd.* **2003**, *353*, 322–326. [CrossRef]
36. Zhang, Y.; Han, X.; Li, B.; Ren, H.; Dong, X.; Wang, X. Electrochemical characteristics of $Mg_{2-x}Zr_xNi$ (x=0–0.6) electrode alloys prepared by mechanical alloying. *J. Alloy. Compd.* **2008**, *450*, 208–214. [CrossRef]
37. Woo, J.H.; Jung, C.B.; Lee, J.H.; Lee, K.S. Electrochemical characteristics of nanocrystalline $ZrCr_2$ and Mg_2Ni type metal hydrides prepared by mechanical alloying. *J. Alloy. Compd.* **1999**, *293–295*, 556–563. [CrossRef]
38. Anik, M.; Akay, I.; Özdemir, G.; Baksan, B. Electrochemical hydrogen storage performance of Mg–Ti–Zr–Ni alloys. *Int. J. Hydrogen Energy* **2009**, *34*, 9765–9772. [CrossRef]
39. Kohno, T.; Yamamoto, M.; Kanda, M. Electrochemical properties of mechanically ground Mg_2Ni alloy. *J. Alloy. Compd.* **1999**, *293–295*, 643–647. [CrossRef]
40. Hou, X.J.; Kou, H.C.; Zhang, T.B.; Hu, R.; Li, J.S.; Xue, X.Y. First-principles studies on the structures and properties of Ti- and Zn-substituted Mg_2Ni hydrogen storage alloys and their hydrides. *Mater. Sci. Forum* **2013**, *743–744*, 44–52. [CrossRef]
41. Anik, M. Improvement of the electrochemical hydrogen storage performance of magnesium based alloys by various additive elements. *Int. J. Hydrogen Energy* **2012**, *37*, 1905–1911. [CrossRef]
42. Huang, L.W.; Elkedim, O.; Nowak, M.; Chassagnon, R.; Jurczyk, M. $Mg_{2-x}Ti_xNi$ (x=0, 0.5) alloys prepared by mechanical alloying for electrochemical hydrogen storage: Experiments and first-principles calculations. *Int. J. Hydrogen Energy* **2012**, *37*, 14248–14256. [CrossRef]
43. Huang, L.W.; Elkedim, O.; Nowak, M.; Jurczyk, M.; Chassagnon, R.; Meng, D.W. Synergistic effects of multiwalled carbon nanotubes and Al on the electrochemical hydrogen storage properties of Mg_2Ni-type alloy prepared by mechanical alloying. *Int. J. Hydrogen Energy* **2012**, *37*, 1538–1545. [CrossRef]
44. Zeng, Y.; Fan, K.; Li, X.; Xu, B.; Gao, X.; Meng, L. First-principles studies of the structures and properties of Al- and Ag-substituted Mg_2Ni alloys and their hydrides. *Int. J. Hydrogen Energy* **2010**, *35*, 10349–10358. [CrossRef]
45. Wang, L.; Tang, Y.; Wang, Y.; Li, Q.; Song, H.; Yang, H. The hydrogenation properties of $Mg_{1.8}Ag_{0.2}Ni$ alloy. *J. Alloy. Compd.* **2002**, *336*, 297–300. [CrossRef]
46. Xie, Zh.; Fu, A.; Chen, Y.; Pan, F.; Ding, P. Effect of Al addition on microstructure and hydrogen diffusion capability of Mg_2Ni alloy. *J. Funct. Mater.* **2006**, *37*, 601–603. (In Chinese) [CrossRef]
47. Xie, Zh.; Pan, F.; Xiang, Y.; Chen, Y. Synergistic effects of Al and Cr addition on microstructure of Mg_2Ni hydrogen storage alloy. *Mater. Sci. Forum* **2009**, *610–613*, 960–963. [CrossRef]
48. Kohno, T.; Kanda, M. Effect of partial substitution on hydrogen storage properties of Mg_2Ni alloy. *J. Electrochem. Soc.* **1997**, *144*, 2384–2388. [CrossRef]
49. Chen, Y.; Tang, T.; Fu, J.; Pan, F.; Deng, Sh.; Li, J.; Zhao, G. The effect of Al addition on hydrogenation properties of Mg_2Ni alloy. *Mater. Rev.* **2007**, *21*, 194–195, 207. (In Chinese)
50. Shi, H.; Meng, L.; Li, X.; Zheng, S.H. Overviews of element partial substitution study of Mg–Ni-based hydrogen storage material. *J. Handan Coll.* **2010**, *20*, 51–57. (In Chinese) [CrossRef]
51. Xue, J.; Li, G.; Hu, Y. Study on Electrochemical performances of Mg_2Ni system hydrogen storage alloys (in Chinese). *Chin. J. Rare Met.* **2000**, *24*, 128–130. [CrossRef]
52. Huot, J.; Liang, G.; Boily, S.; Van Neste, A.; Schulz, R. Hydrogen storage properties of nanocrystalline $Mg_{1.9}Ti_{0.1}Ni$ made by mechanical alloying. *J. Alloy. Compd.* **1999**, *282*, 286–290. [CrossRef]

53. Iwakura, C.; Shin-ya, R.; Miyanohara, K.; Nohara, S.; Inoue, H. Effects of Ti–V substitution on electrochemical and structural characteristics of MgNi alloy prepared by mechanical alloying. *Electrochim. Acta* **2001**, *46*, 2781–2786. [CrossRef]
54. Orimo, S.; Fujii, H. Materials science of Mg–Ni-based new hydrides. *Appl. Phys. A* **2001**, *72*, 167–186. [CrossRef]
55. Chen, Y.; Miao, H.; Ding, P. Recent Development of element partial substitution to improve the characteristics of Mg–Ni-based hydrogen storage alloys. *Mater. Rev.* **2004**, *18*, 29–33. (In Chinese) [CrossRef]
56. Goo, N.; Lee, K. The electrochemical hydriding properties of Mg–Ni–Zr amorphous alloy. *Int. J. Hydrogen Energy* **2002**, *27*, 433–438. [CrossRef]
57. Feng, Y.; Yuan, H.; Qiao, L.; Liu, Q. Preparation and electrochemical characteristics of $Mg_{0.9}M_{0.1}Ni$(M = Cr, A1, Ti, Zr). *Acta Sci. Nat. Univ. Nankaiensis (Nat. Sci. Ed.)* **2005**, *38*, 74–79. (In Chinese) [CrossRef]
58. Wang, Y.T.; Wan, C.B.; Wang, R.L.; Meng, X.H.; Huang, M.F.; Ju, X. Effect of Cr substitution by Ni on the cycling stability of Mg_2Ni alloy using EXAFS. *Int. J. Hydrogen Energy* **2014**, *39*, 14858–14867. [CrossRef]
59. Liang, G.X.; Boily, S.; Huot, J.; Van Neste, A.; Schulz, R. Hydrogen storage properties of nanocrystalline $Mg_2Ni_xCu_{1-x}$ synthesized by mechanical alloying. *Mater. Sci. Forum* **1998**, *269–272*, 1049–1054. [CrossRef]
60. Zhang, Y.; Li, B.; Ma, Z.; Guo, S.; Qi, Y.; Wang, X. Improved hydrogen storage behaviours of nanocrystalline and amorphous Mg_2Ni-type alloy by Mn substitution for Ni. *Int. J. Hydrogen Energy* **2010**, *35*, 11966–11974. [CrossRef]
61. Zhang, Y.; Zhang, H.; Ding, X.; Liu, D.; Zhang, Q.; Si, T. Microstructure characterization and hydrogen storage properties study of $Mg_2Ni_{0.92}M_{0.08}$ (M = Ti, V, Fe or Si) alloys. *Prog. Nat. Sci. Mater. Int.* **2018**, *28*, 464–469. [CrossRef]
62. Huang, L.W.; Elkedim, O.; Jarzebski, M.; Hamzaoui, R.; Jurczyk, M. Structural characterization and electrochemical hydrogen storage properties of $Mg_2Ni_{1-x}Mn_x$ (x=0, 0.125, 0.25, 0.375) alloys prepared by mechanical alloying. *Int. J. Hydrogen Energy* **2010**, *35*, 6794–6803. [CrossRef]
63. Huang, L.W.; Elkedim, O.; Moutarlier, V. Synthesis and characterization of nanocrystalline Mg_2Ni prepared by mechanical alloying: Effects of substitution of Mn for Ni. *J. Alloy. Compd.* **2010**, *504*, S311–S314. [CrossRef]
64. Yang, H.; Yuan, H.; Ji, J.; Sun, H.; Zhou, Z.; Zhang, Y. Characteristics of $Mg_2Ni_{0.75}M_{0.25}$ (M=Ti, Cr, Mn, Fe, Co, Ni, Cu and Zn) alloys after surface treatment. *J. Alloy. Compd.* **2002**, *330–332*, 640–644. [CrossRef]
65. Zhang, Y.; Yang, H.; Yuan, H.; Yang, E.; Zhou, Z.; Song, D. Dehydriding properties of ternary $Mg_2Ni_{(1-x)}Zr_x$ hydrides synthesized by ball milling and annealing. *J. Alloy. Compd.* **1998**, *269*, 278–283. [CrossRef]
66. Zaluski, L.; Zaluska, A.; Tessier, P.; Ström-Olsen, J.O.; Schulz, R. Catalytic effect of Pd on hydrogen absorption in mechanically alloyed Mg_2Ni, $LaNi_5$ and FeTi. *J. Alloy. Compd.* **1995**, *217*, 295–300. [CrossRef]
67. Janot, R.; Aymard, L.; Rougier, A.; Nazri, G.A.; Tarascon, J.M. Fast hydrogen sorption kinetics for ball-milled Mg_2Ni alloys. *J. Phys. Chem. Solids* **2004**, *65*, 529–534. [CrossRef]
68. Chen, Y.; Tang, T.; Fu, J.; Pan, F.; Deng, Sh.; Li, J.; Zhao, G. The effect of Cu addition on hydrogenation properties of Mg_2Ni alloy. *J. Funct. Mater.* **2007**, *38*, 952–954. (In Chinese) [CrossRef]
69. Chen, Y.; Huang, H.; Fu, J.; Guo, Q.; Pan, F.; Deng, Sh.; Li, J.; Zhao, G. Hydrogen storage properties of $Mg_2Ni_{1-x}Cu_x$ (x=0, 0.2, 0.4) synthesized by induction melting followed by ball milling. *Rare Met. Mat. Eng.* **2010**, *39*, 149–152. (In Chinese)
70. Wang, X.; Tu, J.; Zhang, X.; Rong, W.; Chen, Ch. Hydrogen storage properties of tetragonal nanocrystalline $Mg_{2-x}Ti_xNi_{0.8}Cr_{0.2}$ alloy. *Chin. J. Nonferr. Met.* **2004**, *14*, 1020–1024. (In Chinese) [CrossRef]
71. Duan, R. Synthesis and hydrogen storage properties of Mg-based Mg_2Ni type $Mg_{(2-x)}Al_xNi_{(1-y)}Co_y$ hydrogen storage alloys. Master's Thesis, Inner Mongolia Normal University, Huhhot, China, May 2017. (In Chinese)
72. Sun, H.; Feng, D.; Zhang, Y.; Ren, H. Gas hydrogen absorption and electrochemical properties of $Mg_{24}Ni_{10}Cu_2$ alloys improved by Y substitution, ball milling and Ni addition. *Int. J. Hydrogen Energy* **2018**, *44*, 5382–5388. [CrossRef]
73. Li, Y.; Zhang, Y.; Kong, X.; Ding, Y.; Zhang, R.; Tang, J. Thermal stability of the Mg_2Ni-based hydrogen storage alloy doped Ti element. *Int. J. Heat Technol.* **2016**, *34*, 245–250. [CrossRef]
74. Liu, Zh.; Zhu, Y.; Yang, Y.; Gu, H.; Li, L. Influence of vanadium on hydrogen storage properties of Mg-Based alloys. *Chin. J. Rare Met.* **2010**, *34*, 807–811. (In Chinese)
75. Li, Y.; Hou, H.; Zhao, Y.; Yang, L.; Wang, N. Effects of Ti alloying on the Mg_2Ni hydrogen storage alloy (in Chinese). *Special Casting & Nonferrous Alloy.* **2016**, *36*, 341–344. [CrossRef]

76. Wang, Zh.; Zhao, D.; Hou, Zh.; Yong, H.; Zhang, Y.; Wang, X. Hydrogen storage characteristics of ball-milling Mg_2Ni_{50}+*x*wt%Ti (x=0,1,3,5) alloys. *Met. Funct. Mater.* **2011**, *18*, 15–19. (In Chinese)
77. Wang, H.; Nian, H.; Ren, X.; Li, X.; Zhou, Y. Hydrogen desorption properties of reactive ball milled Mg-Ni-M (M =Ni, Nb, Y, Ti) composite materials. *Powder Metall. Technol.* **2011**, *29*, 259–262. (In Chinese)
78. Grigorova, E.; Khristov, M.; Khrussanova, M.; Bobet, J.L.; Peshev, P. Effect of additives on the hydrogen sorption properties of mechanically alloyed composites based on Mg and Ni. *Int. J. Hydrogen Energy* **2005**, *30*, 1099–1105. [CrossRef]
79. Zhao, X.; Li, Q.; Lin, G.; Zhou, G.; Zhang, J.; Lu, X. Hydriding reaction kinetics of Mg–$Mg_2Ni_{(1-x)}Me_x$ compositions. *Chin. J. Nonferr. Met.* **2008**, *18*, 873–878. (In Chinese) [CrossRef]
80. Sun, H.; Feng, D.; Ren, H.; Zhang, Y. Hydrogen storage properties of $Mg_{22}Y_2Ni_{10}Cu_2$+*x*% Ni composite prepared by ball milling. *Chin. J. Rare Met.* **2018**, *42*, 14–20. (In Chinese) [CrossRef]
81. Zhang, Y.; Chen, L.; Lei, Y.; Wang, Q. The reduction of cycling capacity degradation of Mg–Ni-based electrode alloys by Fe substitution. *Int. J. Hydrogen Energy* **2002**, *27*, 501–506. [CrossRef]
82. Ye, H.; Chen, L.; Lei, Y. Effect of nickel on the structure and electrochemical properties of mechanically alloyed Mg–Ni based binary hydrogen storage alloys. *Rare Met. Mat. Eng.* **2000**, *29*, 193–196. (In Chinese) [CrossRef]
83. Bhatnagar, A.; Johnson, J.K.; Shaz, M.A.; Srivastava, O.N. TiH_2 as a dynamic additive for improving the de/rehydrogenation properties of MgH_2: A combined experimental and theoretical mechanistic investigation. *J. Phys. Chem. C* **2018**, *122*, 21248–21261. [CrossRef]
84. Zhou, C.; Li, C.; Li, Y.; Zhang, Q. Enhanced hydrogen storage kinetics of an Mg–Pr–Al composite by in situ formed Pr_3Al_{11} nanoparticles. *Dalton Trans.* **2019**, *48*, 7735–7742. [CrossRef] [PubMed]
85. Korablov, D.; Besenbacher, F.; Jensen, T.R. Kinetics and thermodynamics of hydrogenation-dehydrogenation for Mg-25%TM (TM=Ti, Nb or V) composites synthesized by reactive ball milling in hydrogen. *Int. J. Hydrogen Energy* **2018**, *43*, 16804–16814. [CrossRef]
86. Liang, G.; Huot, J.; Boily, S.; Van Neste, A.; Schulz, R. Catalytic effect of transition metals on hydrogen sorption in nanocrystalline ball milled MgH_2–Tm (Tm=Ti, V, Mn, Fe and Ni) systems. *J. Alloy. Compd.* **1999**, *292*, 247–252. [CrossRef]
87. Polanski, M.; Nawra, D.; Zasada, D. Mg_2FeH_6 synthesized from plain steel and magnesium hydride. *J. Alloy. Compd.* **2019**, *776*, 1029–1040. [CrossRef]
88. Khan, D.; Zou, J.; Zeng, X.; Ding, W. Hydrogen storage properties of nanocrystalline Mg_2Ni prepared from compressed 2MgH_2–Ni powder. *Int. J. Hydrogen Energy* **2018**, *43*, 22391–22400. [CrossRef]
89. Park, H.R.; Kwon, S.N.; Song, M.Y. Effects of milling time on the hydrogen storage properties of Mg-based transition metals-added alloys. *Mater Sci.* **2018**, *24*, 166–171. [CrossRef]
90. Liang, G.; Huot, J.; Boily, S.; Van Neste, A.; Schulz, R. Hydrogen storage properties of the mechanically milled MgH_2–V nanocomposite. *J. Alloy. Compd.* **1999**, *291*, 295–299. [CrossRef]
91. Pelletier, J.F.; Huot, J.; Sutton, M.; Schulz, R.; Sandy, A.R.; Lurio, L.B.; Mochrie, S.G.J. Hydrogen desorption mechanism in MgH_2–Nb nanocomposites. *Phys. Rev. B* **2001**, *63*, 811–820. [CrossRef]
92. Huot, J.; Pelletier, J.F.; Liang, G.; Sutton, M.; Schulz, R. Structure of nanocomposite metal hydrides. *J. Alloy. Compd.* **2002**, *330–332*, 727–731. [CrossRef]
93. Huot, J.; Pelletier, J.F.; Lurio, L.B.; Sutton, M.; Schulz, R. Investigation of dehydrogenation mechanism of MgH_2–Nb nanocomposites. *J. Alloy. Compd.* **2003**, *348*, 319–324. [CrossRef]
94. De Castro, J.F.R.; Santos, S.F.; Costa, A.L.M.; Yavari, A.R.; Botta, W.J.; Ishikawa, T.T. Structural characterization and dehydrogenation behavior of Mg–5at%Nb nanocomposite processed by reactive milling. *J. Alloy. Compd.* **2004**, *376*, 251–256. [CrossRef]
95. Zhong, H.; Lai, G.; Zhu, Z.; Zheng, Q. Hydrogen Storage Properties and mechanism of Mg–In–Zn ternary solid solution by ball milling. *J. Lujiang Univ.* **2014**, *22*, 17–21. (In Chinese) [CrossRef]
96. Janot, R.; Rougier, A.; Aymard, L.; Lenain, C.; Herrera-Urbina, R.; Nazri, G.A.; Tarascon, J.M. Enhancement of hydrogen storage in MgNi by Pd-coating. *J. Alloy. Compd.* **2003**, *356–357*, 438–441. [CrossRef]
97. Lee, D.; Kwon, I.; Bobet, J.L.; Song, M. Effect on the H_2-sorption properties of Mg of Co (with various sizes) and CoO addition by reactive grinding. *J. Alloy. Compd.* **2004**, *366*, 279–288. [CrossRef]
98. Luo, Y.; Meng, Ch.; Xu, Sh.; Feng, C.; Kang, L. Microstructure and hydrogen storage performance of alloys $Mg_xTi_{(100-x)}$ prepared by high-energy ball milling. *J. Lanzhou Univ. Technol.* **2011**, *37*, 9–13. (In Chinese) [CrossRef]

99. Ying, Y.; Zeng, X.; Chang, J.; Zou, J.; Ding, W. Research progress of catalysts for Mg-based hydrogen storage materials. *Mater. Rev.* **2011**, *25*, 134–138. (In Chinese)
100. Liu, M.; Zhang, M.; Huo, Y.; Yan, Sh.; Zhang, H.; Sun, G. Study on modification of Mg-based hydrogen storage materials. *Mater. Res. Appl.* **2013**, *7*, 143–146. (In Chinese) [CrossRef]
101. Chen, M.; Xiao, X.; Zhang, M.; Liu, M.; Huang, X.; Zheng, J.; Zhang, Y.; Jiang, L.; Chen, L. Excellent synergistic catalytic mechanism of in-situ formed nanosized Mg_2Ni and multiple valence titanium for improved hydrogen desorption properties of magnesium hydride. *Int. J. Hydrogen Energy* **2019**, *44*, 1750–1759. [CrossRef]
102. Liu, P.; Chen, H.; Yu, H.; Liu, X.; Jiang, R.; Li, X.; Zhou, S. Oxygen vacancy in magnesium/cerium composite from ball milling for hydrogen storage improvement. *Int. J. Hydrogen Energy* **2019**, *44*, 13606–13612. [CrossRef]
103. Webb, C.J. A review of catalyst-enhanced magnesium hydride as a hydrogen storage material. *J. Phys. Chem. Solids* **2015**, *84*, 96–106. [CrossRef]
104. Zhang, X.; Leng, Z.; Gao, M.; Hu, J.; Du, F.; Yao, J.; Pan, H.; Liu, Y. Enhanced hydrogen storage properties of MgH_2 catalyzed with carbon-supported nanocrystalline TiO_2. *J. Power Sour.* **2018**, *398*, 183–192. [CrossRef]
105. El-Eskandarany, M.S.; Al-Nasrallah, E.; Banyan, M.; Al-Ajmi, F. Bulk nanocomposite MgH_2/10wt%(8 Nb_2O_5/2 Ni) solid-hydrogen storage system for fuel cell applications. *Int. J. Hydrogen Energy* **2018**, *43*, 23382–23396. [CrossRef]
106. Daryani, M.; Simchi, A.; Sadati, M.; Hosseini, H.M.; Targholizadeh, H.; Khakbiz, M. Effects of Ti-based catalysts on hydrogen desorption kinetics of nanostructured magnesium hydride. *Int. J. Hydrogen Energy* **2014**, *39*, 21007–21014. [CrossRef]
107. AGUEYZINSOU, K.; ARESFERNANDEZ, J.; KLASSEN, T.; BORMANN, R. Effect of Nb_2O_5 on MgH_2 properties during mechanical milling. *Int. J. Hydrogen Energy* **2007**, *32*, 2400–2407. [CrossRef]
108. Oelerich, W.; Klassen, T.; Bormann, R. Metal oxides as catalysts for improved hydrogen sorption in nanocrystalline Mg-based materials. *J. Alloy. Compd.* **2001**, *315*, 237–242. [CrossRef]
109. Wang, P.; Wang, A.M.; Zhang, H.F.; Ding, B.Z.; Hu, Z.Q. Hydrogenation characteristics of Mg–TiO_2 (rutile) composite. *J. Alloy. Compd.* **2000**, *313*, 218–223. [CrossRef]
110. Kwon, I.H.; Bobet, J.L.; Bae, J.S.; Song, M.Y. Improvement of hydrogen-storage properties of Mg by reactive mechanical grinding with Fe_2O_3. *J. Alloy. Compd.* **2005**, *396*, 264–268. [CrossRef]
111. Dehouche, Z.; Klassen, T.; Oelerich, W.; Goyette, J.; Bose, T.K.; Schulz, R. Cycling and thermal stability of nanostructured MgH_2∓Cr_2O_3 composite for hydrogen storage. *J. Alloy. Compd.* **2002**, *347*, 319–323. [CrossRef]
112. Barkhordarian, G.; Klassen, T.; Bormann, R. Fast hydrogen sorption kinetics of nanocrystalline Mg using Nb_2O_5 as catalyst. *Scr. Mater.* **2003**, *49*, 213–217. [CrossRef]
113. Hanada, N.; Ichikawa, T.; Hino, S.; Fujii, H. Remarkable improvement of hydrogen sorption kinetics in magnesium catalyzed with Nb_2O_5. *J. Alloy. Compd.* **2006**, *420*, 46–49. [CrossRef]
114. Jung, K.S.; Lee, E.Y.; Lee, K.S. Catalytic effects of metal oxide on hydrogen absorption of magnesium metal hydride. *J. Alloy. Compd.* **2006**, *421*, 179–184. [CrossRef]
115. Liu, Z.; Lei, Zh. Cyclic hydrogen storage properties of Mg milled with nickel nano-powders and MnO_2. *J. Alloy. Compd.* **2007**, *443*, 121–124. [CrossRef]
116. Oelerich, W.; Klassen, T.; Bormann, R. Hydrogen sorption of nanocrystalline Mg at reduced temperatures by metal-oxide catalysts. *Adv. Eng. Mater.* **2001**, *3*, 487–490. [CrossRef]
117. Castro, F.J.; Bobet, J.L. Hydrogen sorption properties of an Mg + WO_3 mixture made by reactive mechanical alloying. *J. Alloy. Compd.* **2004**, *366*, 303–308. [CrossRef]
118. Yu, Zh.; Wang, E.; Liu, Z. Hydorgen storage properties of nanocomposite Mg–Ni–V_2O_5. *J. Funct. Mater.* **2002**, *33*, 280–282. (In Chinese) [CrossRef]
119. Yu, Zh.; Wang, E.; Liu, Z.; Xian, H. Properties of hydriding and dehydriding of nanocrystalline composite of Mg–Ni–Cr_2O_3. *Chin. J. Nonferr. Met.* **2002**, *12*, 743–748. (In Chinese) [CrossRef]
120. Song, M.; Bobet, J.L.; Darriet, B. Improvement in hydrogen sorption properties of Mg by reactive mechanical grinding with Cr_2O_3, Al_2O_3 and CeO_2. *J. Alloy. Compd.* **2002**, *340*, 256–262. [CrossRef]
121. Barkhordarian, G.; Klassen, T.; Bormann, R. Effect of Nb_2O_5 content on hydrogen reaction kinetics of Mg. *J. Alloy. Compd.* **2004**, *364*, 242–246. [CrossRef]

122. Friedrichs, O.; Sanchez-Lopez, J.C.; López-Cartes, C.; Klassen, T.; Bormann, R.; Fernández, A. Nb_2O_5 "Pathway Effect" on Hydrogen Sorption in Mg. *J. Phys. Chem. B* **2006**, *110*, 7845–7850. [CrossRef] [PubMed]
123. Jangir, M.; Jain, A.; Yamaguchi, S.; Ichikawa, T.; Lal, C.; Jain, I.P. Catalytic effect of TiF_4 in improving hydrogen storage properties of MgH_2. *Int. J. Hydrogen Energy* **2016**, *41*, 14178–14183. [CrossRef]
124. Bhat, V.V.; Rougier, A.; Aymard, L.; Darok, X.; Nazri, G.; Tarascon, J.M. Catalytic activity of oxides and halides on hydrogen storage of MgH_2. *J. Power Sour.* **2006**, *159*, 107–110. [CrossRef]
125. Yahya, M.S.; Sulaiman, N.N.; Mustafa, N.S.; Halim Yap, F.A.; Ismail, M. Improvement of hydrogen storage properties in MgH_2 catalysed by K_2NiF_7. *Int. J. Hydrogen Energy* **2018**, *43*, 14532–14540. [CrossRef]
126. Kim, J.W.; Ahn, J.P.; Jin, S.A.; Lee, S.H.; Chung, H.S.; Shim, J.H.; Cho, Y.W.; Oh, K.H. Microstructural evolution of NbF_2-doped MgH_2 exhibiting fast hydrogen sorption kinetics. *J. Power Sour.* **2008**, *178*, 373–378. [CrossRef]
127. Peng, S.; Xiao, X.; Xu, R.; Li, L.; Wu, F.; Li, S.; Wang, Q.; Chen, L. Hydrogen storage behaviors and microstructure of MF_3 (M=Ti, Fe)-doped magnesium hydride. *Trans. Nonferr. Met. Soc.* **2010**, *20*, 1879–1884. [CrossRef]
128. Yin, Y.; Li, B.; Yuan, Z.; Qi, Y.; Zhang, Y. A comparison of TiF_3 and NbF_5 catalytic effects on hydrogen absorption and desorption kinetics of a ball-milled $Mg_{85}Zn_5Ni_{10}$ alloy. *RSC Adv.* **2018**, *8*, 34525–34535. [CrossRef]
129. Jin, S.A.; Shim, J.H.; Cho, Y.W.; Yi, K.W. Dehydrogenation and hydrogenation characteristics of MgH_2 with transition metal fluorides. *J. Power Sour.* **2007**, *172*, 859–862. [CrossRef]
130. Jin, S.A.; Shim, J.H.; Ahn, J.P.; Cho, Y.W.; Yi, K.W. Improvement in hydrogen sorption kinetics of MgH_2 with Nb hydride catalyst. *Acta Mater.* **2007**, *55*, 5073–5079. [CrossRef]
131. Varin, R.A.; Czujko, T.; Wronski, Z. Particle size, grain size and γ-MgH_2 effects on the desorption properties of nanocrystalline commercial magnesium hydride processed by controlled mechanical milling. *Nanotechnology* **2006**, *17*, 3856–3865. [CrossRef]
132. Luo, Y.; Wang, P.; Ma, L.; Cheng, H. Hydrogen sorption kinetics of MgH_2 catalyzed with NbF_5. *J. Alloy. Compd.* **2008**, *453*, 138–142. [CrossRef]
133. Recham, N.; Bhat, V.V.; Kandavel, M.; Aymard, L.; Tarascon, J.M.; Rougier, A. Reduction of hydrogen desorption temperature of ball-milled MgH_2 by NbF_5 addition. *J. Alloy. Compd.* **2008**, *464*, 377–382. [CrossRef]
134. Malka, I.E.; Czujko, T.; Bystrzycki, J. Catalytic effect of halide additives ball milled with magnesium hydride. *Int. J. Hydrogen Energy* **2010**, *35*, 1706–1712. [CrossRef]
135. De Castro, J.F.R.; Yavari, A.R.; LeMoulec, A.; Ishikawa, T.T.; Botta, F.W.J. Improving H-sorption in MgH_2 powders by addition of nanoparticles of transition metal fluoride catalysts and mechanical alloying. *J. Alloy. Compd.* **2005**, *389*, 270–274. [CrossRef]
136. Deledda, S.; Borissova, A.; Poinsignon, C.; Botta, W.J.; Dornheim, M.; Klassen, T. H-sorption in MgH_2 nanocomposites containing Fe or Ni with fluorine. *J. Alloy. Compd.* **2005**, *404–406*, 409–412. [CrossRef]
137. Malka, I.E.; Pisarek, M.; Czujko, T.; Bystrzycki, J. A study of the ZrF_4, NbF_5, TaF_5, and $TiCl_3$ influences on the MgH_2 sorption properties. *Int. J. Hydrogen Energy* **2011**, *36*, 12909–12917. [CrossRef]
138. Ma, L.P.; Kang, X.D.; Dai, H.B.; Liang, Y.; Fang, Z.Z.; Wang, P.J.; Wang, P.; Cheng, H.M. Superior catalytic effect of TiF_3 over $TiCl_3$ in improving the hydrogen sorption kinetics of MgH_2: Catalytic role of fluorine anion. *Acta Mater.* **2009**, *57*, 2250–2258. [CrossRef]
139. Ivanov, E.; Konstanchuk, I.; Bokhonov, B.; Boldyrev, V.V. Hydrogen interaction with mechanically alloyed magnesium-salt composite materials. *J. Metastab. Nanocryst. Mater.* **2003**, *15–16*, 579–584. [CrossRef]
140. Tian, M.; Shang, C. Mg-based composites for enhanced hydrogen storage performance. *Int. J. Hydrogen Energy* **2019**, *44*, 338–344. [CrossRef]
141. Thongtan, P.; Dansirima, P.; Thiangviriya, S.; Thaweelap, N.; Suthummapiwat, A.; Plerdsranoy, P.; Utke, R. Reversible hydrogen sorption and kinetics of hydrogen storage tank based on MgH_2 modified by TiF_4 and activated carbon. *Int. J. Hydrogen Energy* **2018**, *43*, 12260–12270. [CrossRef]
142. Alsabawi, K.; Webb, T.A.; Gray, E.M.; Webb, C.J. The effect of C_{60} additive on magnesium hydride for hydrogen storage. *Int. J. Hydrogen Energy* **2015**, *40*, 10508–10515. [CrossRef]
143. Yahya, M.S.; Ismail, M. Improvement of hydrogen storage properties of MgH_2 catalyzed by K_2NiF_7 and multiwall carbon nanotube. *J. Phys. Chem. C* **2018**, *122*, 11222–11233. [CrossRef]

144. Popilevsky, L.; Skripnyuk, V.M.; Beregovsky, M.; Sezen, M.; Amouyal, Y.; Rabkin, E. Hydrogen storage and thermal transport properties of pelletized porous Mg-2 wt.% multiwall carbon nanotubes and Mg-2 wt.% graphite composites. *Int. J. Hydrogen Energy* **2016**, *41*, 14461–14474. [CrossRef]
145. Rud, A.D.; Lakhnik, A.M. Effect of carbon allotropes on the structure and hydrogen sorption during reactive ball-milling of Mg–C powder mixtures. *Int. J. Hydrogen Energy* **2012**, *37*, 4179–4187. [CrossRef]
146. Popilevsky, L.; Skripnyuk, V.M.; Amouyal, Y.; Rabkin, E. Tuning the thermal conductivity of hydrogenated porous magnesium hydride composites with the aid of carbonaceous additives. *Int. J. Hydrogen Energy* **2017**, *42*, 22395–22405. [CrossRef]
147. Spassov, T.; Zlatanova, Z.; Spassova, M.; Todorova, S. Hydrogen sorption properties of ball-milled Mg–C nanocomposites. *Int. J. Hydrogen Energy* **2010**, *35*, 10396–10403. [CrossRef]
148. Alsabawi, K.; Gray, E.M.; Webb, C.J. The effect of ball-milling gas environment on the sorption kinetics of MgH_2 with/without additives for hydrogen storage. *Int. J. Hydrogen Energy* **2019**, *44*, 2976–2980. [CrossRef]
149. Yu, Zh.; Sun, H.; Wang, E.; Liang, J.; Fang, W. Hydrogen storage properties of Mg-based materials with CNTs. *Chin. J. Nonferr. Met.* **2005**, *15*, 876–881. (In Chinese) [CrossRef]
150. Yao, Y.; Zhang, S.; Yan, Y. Ball milling process and its effect on hydrogen adsorption storage of MWNTS. *Chin. J. Process. Eng.* **2006**, *6*, 837–840. (In Chinese) [CrossRef]
151. Chen, D.; Chen, L.; Liu, S.; Ma, C.X.; Chen, D.M.; Wang, L.B. Microstructure and hydrogen storage property of Mg/MWNTs composites. *J. Alloy. Compd.* **2004**, *372*, 231–237. [CrossRef]
152. Bouaricha, S.; Dodelet, J.P.; Guay, D.; Huot, J.; Schulz, R. Study of the activation process of Mg-based hydrogen storage materials modified by graphite and other carbonaceous compounds. *J. Mater. Res.* **2001**, *16*, 2893–2905. [CrossRef]
153. Wu, C.Z.; Wang, P.; Yao, X.; Liu, C.; Chen, D.M.; Lu, G.Q.; Cheng, H.M. Effect of carbon/noncarbon addition on hydrogen storage behaviors of magnesium hydride. *J. Alloy. Compd.* **2006**, *414*, 259–264. [CrossRef]
154. Wu, C.; Wang, P.; Yao, X.; Liu, C.; Chen, D.; Lu, G.Q.; Cheng, H. Effects of SWNT and metallic catalyst on hydrogen absorption/desorption performance of MgH_2. *J. Phys. Chem. B* **2005**, *109*, 22217–22221. [CrossRef]
155. Wu, C.Z.; Wang, P.; Yao, X.; Liu, C.; Chen, D.M.; Lu, G.Q.; Cheng, H.M. Hydrogen storage properties of MgH_2/SWNT composite prepared by ball milling. *J. Alloy. Compd.* **2006**, *420*, 278–282. [CrossRef]
156. Zhou, S.; Yang, M.; Ma, H.; Zhang, T.; Zhang, G. The effect of microlitic carbon in Mg-based composite hydrogen-stored materials. *J. Shandong Univ. Sci. Technol.* **2009**, *28*, 54–57. (In Chinese) [CrossRef]
157. Zhou, S.; Zhang, X.; Li, T.; Wang, N.; Chen, H.; Zhang, T.; Yu, H.; Niu, H.; Liu, D. Nano-confined magnesium for hydrogen storage from reactive milling with anthracite carbon as milling aid. *Int. J. Hydrogen Energy* **2014**, *39*, 13628–13633. [CrossRef]
158. Lu, G.; Tang, D. Preparation of Mg–C nanocomposite study on phase transformation rate of hydrogen desorption. *Mater. Rev.* **2009**, *23*, 28–30. (In Chinese) [CrossRef]
159. Zhang, J.; Zhu, P.; Mao, C.; Zhou, D. Influence and micro-mechanism of carbon materials doping on dehydrogenation properties of magnesium based hydride. Chin. *J. Nonferr. Met.* **2015**, *25*, 2464–2470. (In Chinese)
160. Yao, X.; Wu, C.Z.; Wang, H.; Cheng, H.M.; Lu, G.Q. Effects of carbon nanotubes and metal catalysts on hydrogen storage in magnesium nanocomposites. *J. Nanosci. Nanotechnol.* **2006**, *6*, 494–498. [CrossRef] [PubMed]
161. Yao, X.; Wu, C.; Du, A.; Zou, J.; Zhu, Z.; Wang, P.; Cheng, H.; Smith, S.; Lu, G. Metallic and carbon nanotube-catalyzed coupling of hydrogenation in magnesium. *J. Am. Chem. Soc.* **2007**, *129*, 15650–15654. [CrossRef] [PubMed]
162. Wu, C.; Cheng, H.M. Effects of carbon on hydrogen storage performances of hydrides. *J. Mater. Chem.* **2010**, *20*, 5390–5400. [CrossRef]
163. Yao, X.; Wu, C.; Du, A.; Liu, G.Q.; Cheng, H.; Smith, S.C.; Zou, J.; He, Y. Mg-based nanocomposites with high capacity and fast kinetics for hydrogen storage. *J. Phys. Chem. B* **2006**, *110*, 11697–11703. [CrossRef]
164. Li, W.; Hu, S.; Hao, Y.; Dai, J.; Wang, Q. Hydrogen storage property of Mg–Ni–CNTs composites. *J. Gansu Sci.* **2009**, *21*, 54–56. (In Chinese) [CrossRef]
165. Wang, J.; Ebner, A.D.; Ritter, J.A. Kinetic behavior of Ti-doped $NaAlH_4$ when cocatalyzed with carbon nanostructures. *J. Phys. Chem. B* **2006**, *110*, 17353–17358. [CrossRef] [PubMed]

166. Pang, Y.; Yuan, T.; Yang, J.; Gao, M.; Pan, H.; Liu, Y.; Zheng, S. In situ formation of Al_3Ti, MgF_2 and Al and their superior synergetic effects on reversible hydrogen storage of MgH_2. *Catal. Today* **2017**, *318*, 107–112. [CrossRef]
167. Cermak, J.; Kral, L.; Roupcova, P. Improved hydrogen sorption kinetics in Mg modified by chosen catalysts. *Int. J. Hydrogen Energy* **2019**, *44*, 8315–8324. [CrossRef]
168. Lototskyy, M.; Goh, J.; Davids, M.W.; Linkov, V.; Khotseng, L.; Ntsendwana, B.; Denys, R.; Yartys, V.A. Nanostructured hydrogen storage materials prepared by high-energy reactive ball milling of magnesium and ferrovanadium. *Int. J. Hydrogen Energy* **2019**, *44*, 6687–6701. [CrossRef]
169. Zhang, X.; Shen, Z.; Jian, N.; Hu, J.; Du, F.; Yao, J.; Gao, M.; Liu, Y.; Pan, H. A novel complex oxide $TiVO_{3.5}$ as a highly active catalytic precursor for improving the hydrogen storage properties of MgH_2. *Int. J. Hydrogen Energy* **2018**, *43*, 23327–23335. [CrossRef]
170. Pighin, S.A.; Capurso, G.; Lo Russo, S.; Peretti, H.A. Hydrogen sorption kinetics of magnesium hydride enhanced by the addition of Zr_8Ni_{21} alloy. *J. Alloy. Compd.* **2012**, *530*, 111–115. [CrossRef]
171. Zaranski, Z.; Czujko, T. The influence of ball milling process on hydrogenation properties of MgH_2–$FeTiH_x$ composites. *J. Alloy. Compd.* **2011**, *509*, S608–S611. [CrossRef]
172. El-Eskandarany, M.S.; Al-Ajmi, F.; Banyan, M. Mechanically-induced catalyzation of MgH_2 powders with Zr_2Ni-Ball Milling Media. *Catalysts* **2019**, *9*, 382. [CrossRef]
173. Zhang, L.; Cai, Z.; Yao, Z.; Ji, L.; Ze, S.; Yan, N.; Zhang, B.; Xiao, B.; Du, J.; Zhu, X.; et al. A striking catalytic effect of facile synthesized $ZrMn_2$ nanoparticles on the de/rehydrogenation properties of MgH_2. *J. Mater. Chem. A* **2019**, *7*, 5626–5634. [CrossRef]
174. Santos, S.F.; Ishikawa, T.T.; Botta, W.J.; Huot, J. MgH_2+FeNb nanocomposites for hydrogen storage. *Mater. Chem. Phys.* **2014**, *147*, 557–562. [CrossRef]
175. Zhou, C.S.; Fang, Z.G.Z.; Sun, P.; Xu, L.; Liu, Y. Capturing low-pressure hydrogen using Ve-Ti-Cr catalyzed magnesium hydride. *J. Power Sour.* **2019**, *423*, 139–147. [CrossRef]
176. Li, F.; Jiang, L.; Du, J.; Wang, Sh.; Liu, X.; Zhan, F. Synthesis and hydrogenation properties of Mg–La–Ni–H system by reactive mechanical alloying. *Int. J. Hydrogen Energy* **2006**, *31*, 581–585. [CrossRef]
177. Liang, G.; Huot, J.; Boily, S.; Van Neste, A.; Schulz, R. Hydrogen storage in mechanically milled Mg–$LaNi_5$ and MgH_2∓$LaNi_5$ composite. *J. Alloy. Compd.* **2000**, *297*, 261–265. [CrossRef]
178. Fu, Y.; Groll, M.; Mertz, R.; Kulenovic, R. Effect of $LaNi_5$ and additional catalysts on hydrogen storage properties of Mg. *J. Alloy. Compd.* **2008**, *460*, 607–613. [CrossRef]
179. Zhou, Ch.; Fang, Z.Z.; Ren, Ch.; Li, J.; Lu, J. Effect of Ti intermetallic catalysts on hydrogen storage properties of magnesium hydride. *J. Phys. Chem. C* **2013**, *117*, 12973–12980. [CrossRef]
180. Ren, Ch.; Fang, Z.Z.; Zhou, Ch.; Lu, J.; Ren, Y.; Zhang, X. Hydrogen storage properties of magnesium hydride with V-based additives. *J. Phys. Chem. C* **2014**, *118*, 21778–21784. [CrossRef]
181. Molinas, B.; Ghilarducci, A.A.; Melnichuk, M.; Corso, H.L.; Peretti, H.A.; Agresti, F.; Bianchin, A.; Lo Russo, S.; Maddalena, A.; Principi, G. Scaled-up production of a promising Mg-based hydride for hydrogen storage. *Int. J. Hydrogen Energy* **2009**, *34*, 4597–4601. [CrossRef]
182. Makihara, Y.; Umeda, K.; Shoji, F.; Kato, K.; Miyairi, Y. Cooperative dehydriding mechanism in a mechanically milled Mg–50mass% $ZrMn_2$ composite. *J. Alloy. Compd.* **2008**, *455*, 385–391. [CrossRef]
183. Wang, P.; Wang, A.; Zhang, H.; Ding, B.; Hu, Z. Hydriding properties of a mechanically milled Mg–50wt.% $ZrFe_{1.4}Cr_{0.6}$ composite. *J. Alloy. Compd.* **2000**, *297*, 240–245. [CrossRef]
184. Wang, Zh.; Gu, Zh.; Cheng, G.; Cheng, J. Influences of the factors on electrochemical characteristics of Mg_2Ni alloys. *Electr. Eng. Mater.* **2003**, *3*, 40–46. (In Chinese) [CrossRef]